UTILIZATION OF WAVE POWER AS A RENEWABLE ENERGY STORAGE FOR ELECTRICITY GENERATION

Rajapaksha Pathiranage Thilanka Sandaruwan Gunawardana

208680A

Master of Science in Electrical Installations

Department of Electrical Engineering

Faculty of Engineering

University of Moratuwa

Sri Lanka

July 2025

UTILIZATION OF WAVE POWER AS A RENEWABLE ENERGY STORAGE FOR ELECTRICITY GENERATION

Rajapaksha Pathiranage Thilanka Sandaruwan Gunawardana

208680A

Thesis/Dissertation submitted in partial fulfillment of the requirements for the degree
Master of Science in Electrical Installations

Department of Electrical Engineering

Faculty of Engineering

University of Moratuwa

Sri Lanka

July 2025

DECLARATION

I declare that this is my own work and this thesis/dissertation does not incorporate without acknowledgement any material previously submitted for a degree or diploma in any other University or Institute of higher learning and to the best of my knowledge and belief it does not contain any material previously published or written by another person except where the acknowledgement is made in the text. I retain the right to use this content in whole or part in future works (such as articles or books).

Signature: Date: 27.07.2025

....

R.P.T.S.Gunawardana

The above candidate has carried out research for the Master's thesis under my supervision. I confirm that the declaration made above by the student is true and correct.

Name of Supervisor:

Prof. W.D.A.S.Wijayapala

…………………………

Signature of the Supervisor: Date:28.07.2025

ACKNOWLEDGEMENT

I hereby express my deepest gratitude and sincere appreciation to my supervisor, Prof. Anura Wijayapala, Head of the Department of Electrical Engineering, Faculty of Engineering, University of Moratuwa, Sri Lanka, for his invaluable guidance, constructive advice, motivation and constant supervision throughout the research study. His academic support and personal encouragement over the past three years have been instrumental in the completion of this work.

I extend my appreciation to Dr. V. Logeeshan for his technical expertise and assistance with the fluid dynamic simulations, as well as to the esteemed faculty members, including professors, senior lecturers, lecturers, and instructors of the Department of Electrical Engineering, University of Moratuwa, for their generous cooperation.

Finally, I must express my heartfelt gratitude to my loving parents and wife for their endless support and sacrifices, without which this achievement would not have been possible.

R.P.T.S.Gunawardana

208680A

ABSTRACT

The growing demand for sustainable energy solutions necessitates innovative approaches to renewable energy extraction and storage. This research introduces a novel concept for wave energy extraction and storage systems as a renewable energy source, utilizing an oscillating floater to produce compressed air for electricity generation.

The study titled “Utilization of wave power as a renewable energy storage for electricity generation” was conducted through two main approaches: (1) designing and simulating a 1 kW pilot wave energy extractor model and (2) constructing the optimum design of the pilot model. The system is designed to extract 1 kW of power from 1 m^2 of the sea wave surface. The parameters 1 m^2 and 1 kW were selected on the basis of maintaining a per-unit value for scaling calculations.

The conceptual design consists of a floating mechanism that captures wave energy through buoyancy. This energy is amplified through a lever system and converted to compressed air via pistons. The compressed air is then stored in accumulators, such that it can be discharged on demand. For a continuous operation, multiple interconnected accumulators can operate in alternating charge-discharge cycles. The released air energy is then captured by an air turbine coupled to an electricity generator.

Given the absence of an exactly similar comparable system, this research was conducted on theoretical calculations, evidence-based assumptions, and iterative trial-and-error methods to achieve the outcome. For the ease of the study, the complete system was executed mainly in two phases, from energy extraction to energy storage and from energy storage to electricity generation.

This innovative approach offers significant potential for harnessing wave energy, one of the most abundant and underutilized renewable resources. By addressing both energy extraction and storage simultaneously, the system provides a comprehensive solution to the untapped potential of wave energy to meet global energy demand.

Keywords: Wave energy, Oscillating floater, Compressed air energy storage, Renewable energy, Energy extraction, Energy conversion, Electricity generation

TABLE OF CONTENTS

LIST OF FIGURES

LIST OF TABLES

LIST OF ABBREVIATIONS

Abbreviation	Description
WEC	Wave Energy Converters
CAES	Compressed Air Energy Storage
PTO	Power Take Off
CFD	Computational Fluid Dynamics
PMAC	Permanent Magnet Alternating Current
PSI	Pounds per Square Inch
CAPEX	Capital Expenditure
OPEX	Operational Expenditure
R&D	Research & Development

LIST OF APPENDICES

CHAPTER 1

INTRODUCTION

1.1 Background

The global energy supply is being challenged by increasing energy demands, depleting fossil fuel reserves, and environmental concerns related to carbon emissions. These challenges have driven research into renewable energy sources as sustainable alternatives to conventional energy sources. Among various renewable energy sources, ocean wave energy represents one of the most abundant and untapped resources, with an estimated global potential of 2 TW, equivalent to approximately 10% of global electricity consumption [1].

Out of the existing renewable sources, wave energy has many advantages. The accuracy of the wave energy prediction is higher than that of other renewable resources. Wave energy has a higher energy density. The variability over time is comparatively low. Besides these advantages, due to technical challenges in efficient harnessing, converting, and storing, the wave energy technologies have lagged behind the other renewables in terms of commercial deployment.

Most traditional wave energy converters (WECs) focus mainly on direct electricity generation without substantial storage facilities. Hence, this would affect the output fluctuations during grid integration. Furthermore, many existing WEC designs are facing durability issues in harsh marine environments. When it tries to mitigate these issues, it leads to high maintenance costs and reduced operational reliability.

Compressed air energy storage (CAES) systems are emerging technologies in the energy sector, which can be introduced as a cost-effective storage solution due to their relatively simple technology, scalability, and potential for high energy density storage. However, the integration of CAES with wave energy conversion systems remains a relatively unexplored territory in the energy storage sector.

This research addresses these gaps by developing an integrated system that combines wave energy extraction with compressed air storage, overcoming the challenges that have limited wave energy utilization in the renewable energy scope.

1.2 Problem statement

The depletion of non-renewable energy sources highly impacts the world's energy demand. Thus, the renewable energy sources such as hydro, wind, and solar play a vital role in serving the incremental demand. But the capacities are limited. However, among the most available renewable energy sources, ocean wave energy has not yet been utilized for energy generation. It is still an abundant and untapped energy source, even though there are small-scale wave energy extractors around the world. Among them, there is no sophisticated methodology to extract wave energy, compress air, store energy, and generate electricity from the compressed air. Therefore, this space is addressed in this research by introducing a design for wave energy extraction, energy storage and electricity generation. The details of designing, simulating and constructing a pilot model are included in this research.

1.3 Research objectives

The research objective of this study is to develop an optimum wave energy extractor through an oscillating floater to produce compressed air and generate electricity. This will be achieved by designing & simulating a 1kW pilot wave energy extractor model and constructing the optimum design of the pilot model.

1.4 Thesis overview

Chapter 2 of this thesis gives a comprehensive literature review on the potential of wave energy and the existing energy extracting technologies. It also presents the detailed reviews regarding the selected methodologies and devices that are to be used in the research.

Chapter 3 describes the methodologies of site selections and the fundamental theories for the calculations of the design, based on which the theoretical model and the pilot model have to be developed.

Chapter 4 focuses on the simulations done for the confirmation of the theoretical model for the development. Chapter 5 presents the pilot model developed based on calculations and simulations. Chapter 6 details the calculations, including energy flow and the results of the design calculations. Finally, Chapter 7 briefs the conclusion and the recommendations of the study.

CHAPTER 2

LITERATURE REVIEW

2.1 Potential of wave energy

Wave energy, derived from ocean surface waves, is the most emerging, abundant, and untapped renewable energy source with a significantly high energy density and predictability compared to wind and solar power. Since 70% of the Earth's surface is covered by oceans, studies have estimated that the worldwide theoretical wave energy resource capacity ranges between 8,000 and 80,000 TWh/year [2]. Furthermore, the coastal wave energy resource has been estimated to exceed 2 TW [3]. Wave energy also claims higher power density compared to other renewables, delivering approximately 2–30 kW/m of wave front, while solar and wind average 100–300 W/m² and 300–1,200 W/m², respectively [3], depending on geographic location and technology efficiency. Coastal regions such as the western shores of Europe, the Pacific Northwest of North America, and southern Australia have been identified as high energy potential areas (Figure 2.1). In Sri Lanka, the southern and western coasts are observed with moderate potential [4].

Figure 2.1: Map of wave energy flux around the world

The main advantages of wave energy can be identified as high availability, high density, predictability, and minimal land use compared to wind and solar. However, challenges such as high maintenance due to harsh marine environments, environmental and navigational concerns, and the immature commercial state of wave technology still hinder widespread deployment [5].

2.2 Wave energy converter technologies

WECs can be deployed in offshore, near-shore, and shoreline configurations, each with distinct advantages and challenges. Offshore systems benefit from higher wave energy, while near-shore and shoreline installations offer easier maintenance and grid connection. WECs can be categorized based on their working principles and design configurations. WEC technologies have advanced significantly, with various designs, such as point absorbers, oscillating water columns, and overtopping devices, demonstrating feasibility in harnessing ocean wave power. Each technology offers distinct advantages in efficiency, scalability, and deployment location, but challenges like structural durability, energy conversion losses, and high capital costs.

2.2.1 Point absorber buoy

A floating structure that moves vertically with wave action, converting the heave motion into electricity through hydraulic pumps or direct-drive generators [6].

- PowerBuoy PB3 (USA, Pacific Ocean off Oregon coast) - 86 kW [7]
- CETO 6 (Australia, Indian Ocean off Garden Island) - 1 MW [8]

2.2.2 Surface attenuator

Long, multi-segment floating devices orientated parallel to wave direction that generate power from the relative motion between sections [9].

- Pelamis P2 (UK, North Sea at EMEC Orkney) - 750 kW [10]
- SeaRAY (USA, Pacific Ocean, Hawaii Test Site) - 50 kW [11]

2.2.3 Oscillating wave surge converter

Fixed or hinged flaps near shore that capture energy from the back-and-forth surge motion of waves [12].

- *Oyster 800* (UK, Atlantic Ocean at EMEC Orkney) - 800 kW [9]
- *OceanEnergy Buoy* (Ireland, Atlantic Ocean off Galway) - 500 kW [13]

2.2.4 Oscillating water column

Partially submerged chambers where wave action compresses air to drive a turbine [14].

- *Mutriku Breakwater Plant* (Spain, Bay of Biscay) - 296 kW [15]
- *LIMPET* (UK, North Atlantic at Islay, Scotland) - 500 kW [16]

2.2.5 Overtopping device

Funnel-shaped structures that capture waves in elevated reservoirs, with water returning through turbines [17].

- *Wave Dragon* (Denmark, North Sea at Nissum Bredning) - 7 MW (prototype) [18]
- *SSG* (Norway, North Sea at Kvitsøy) - 350 kW (pilot) [19]

2.2.6 Submerged pressure differential

Underwater devices that use wave-induced pressure changes to drive power take-off systems [20].

- *Archimedes Wave Swing* (Portugal, Atlantic Ocean off Póvoa de Varzim) - 2 MW [21]
- *WaveRoller* (Finland, Baltic Sea near Península de Peniche) - 1 MW [14]

2.2.7 Floating in-air converters

Tethered systems where wave motion drives airborne components [22].

- *Wavestar Air* (Denmark, North Sea at Hanstholm) - 500 kW (design) [23]
- *Kite Systems* (Sweden, Baltic Sea at Uppsala test site) - 50 kW [24]

2.3 Performance and efficiency of wave energy converters

The overall performance of wave energy converters mainly depends on the method of power capture, environmental conditions, the type of wave energy converter, and efficiency considerations of conversion technologies. The WEC types extract energy through different mechanisms as described in section 2.2. The environmental conditions, such as location (offshore or onshore), wind directions, depth, and seabed topography, impact the variation of the wave height, wave period, and direction.

The fundamental equation of the wave energy flux (wave power per unit width) is used to quantify the available wave energy that a WEC can potentially capture, which represents the energy transferred by ocean waves per meter of wave crest [25]. The wave energy flux in deep water is given by Equation 1.

$$P = \frac{\rho g^2 H^2 T}{64\pi} \qquad \textit{... Equation [1]}$$

Where;

P – Wave power per meter of wave front (kW/m)

P – Sea water density (~1025 kg/m^3)

g – Gravitational acceleration (9.81 m/s^2)

H – Wave height (m)

T–Wave period (s)

Further to the performance, the viability of a wave energy conversion system is determined by the efficiency. Generally, the efficiency of a converter is defined as how much power is absorbed from the available power within the device width [25].

$$Efficiency\ (\eta) = \frac{Power\ Absorbed}{Power\ Available\ Within\ the\ Device\ Width} \qquad \textit{... Equation [2]}$$

The overall efficiency of wave energy converters (WECs) is determined by multiple conversion stages. At each stage, there is a contribution to energy loss in the power transformation process. The efficiencies can be categorized with reference to the multiple stages as hydrodynamic efficiency, mechanical efficiency, and electrical efficiency [25]. The hydrodynamic efficiency is influenced by factors such as device geometry and environmental conditions, which determine how effectively the device captures the wave energy from the waves. Once the energy is extracted, it has to be transformed into mechanical energy through a series of mechanical conversions. Therefore, at these conversion stages, there are losses in moving components like hydraulic systems, gearboxes, levers, pistons, linkages, etc. The net output of the mechanical conversion is considered in mechanical efficiency. The final stage is the efficiency at conversion of mechanical energy into electrical energy for grid compatibility through generators and power electronics. Hence, the overall efficiency can be obtained from Equation 3.

$$\eta_{overall} = \eta_{hydro} \times \eta_{mech} \times \eta_{elec} \qquad \textit{... Equation [3]}$$

Where:

η_{hydro} - Hydrodynamic efficiency (~20–50%)

η_{mech} - Mechanical efficiency (~70–90%)

η_{elec} - Electrical efficiency (~85–95%)

Table 2.1: Efficiencies of ongoing wave energy converter systems

Project Name	**Country**	**Scale**	**Wave Energy Potential**	**Efficiency**
Pelamis	Scotland	Simulation experiments	12 kW/m	21%
Langlee Technology	Norway	Lab experiments	16 kW/m	7%
Wave Piston	Denmark	Simulation	3.5 kW/m	8%
SEAREV	France	Simulation	25 kW/m	20%

Table 2.2: Efficiencies of power take-off methods

PTO Type	**Efficiency (%)**
Hydraulic	65%
Water	85%
Air turbines	55%
Mechanical drive	90%
Direct drive linear generator	95%

Referring to Table 2.1, the overall efficiency of commercially available composite WEC systems is recorded around the range of 8-25%. The most significant energy losses occur during the hydrodynamic and mechanical conversion phases, Table 2.2. Hence, it can be concentrated on research focusing on key improvement areas of the efficiency losses. Mainly, the development of adaptive control systems can be enhanced to capture wave energy, and power take-off mechanisms can be developed to minimize mechanical losses.

2.4 Computational fluid dynamics simulations

Computational Fluid Dynamics (CFD) is used to analyze and solve problems involving fluid flows, heat transfer, and associated phenomena with numerical methods and algorithms. The fluid dynamics related to physical tests can be simulated to check how fluids interact with surfaces under specified conditions by using CFDs. The flow patterns, pressure distributions, turbulence effects, and energy transfers can be visualized prior to executing physical experiments.

In the context of wave energy conversion, CFD is used to model complex interactions between ocean wave propagation, device components such as floaters, and energy transfer mechanisms. Unlike the traditional analytical methods, nonlinear wave effects, turbulence, and viscous losses can be simulated using CFDs.

The main procedures of the CFD simulations are as follows.

1. Geometry modelling of the hull reservoir device
2. Mesh generation with refined zones near moving components
3. Boundary condition setup using wave theories
4. Solver execution with turbulence models
5. Validation against experimental or theoretical data

This approach has enabled the optimization of the WEC's power take-off system and reservoir design while minimizing computational costs [26]. Multi-physics simulation platforms such as SimFlow, Ansys, and COMSOL are commonly used in the research studies.

2.5 Types of air compressors

An air compressor is a device that transfers the kinetic energy of air into potential energy by reducing volume. There are two types of air compressors classified according to their operation as positive displacement compressors and dynamic compressors. In positive displacement compressors, the air is pressurized into a specific volume by methods like reciprocating and rotary screws. These compressors are used for applications that require high pressure and low air flow. In dynamic compressors, the air is pressurized using centrifugal or axial rotating impellers [27]. These dynamic compressors are more suitable for large-scale applications where a continuous high volume of air is required.

2.6 Compressed air energy storage

Compressed air energy storage (CAES) is a technology that stores energy generated at one time for use at another time. At utility scale, energy generated during periods of low energy demand (off-peak) can be released to higher demand (peak load) periods. CAES can be used to balance intermittent renewable energy supply with the grid demand, since it has high capacity, can store for long durations, and offers cost-effective scalability. Underground reservoirs such as salt caverns, depleted gas fields, and pressurized tanks are used to store compressed air.

2.6.1 World history of CAES systems

In 1978, the first large-scale 290 MW CAES plant was opened using a salt cavern in Germany. In 1991, a 110 MW plant was built in McIntosh, Alabama, using a salt cavern. In 2009, a 300 MW plant was built by Pacific Gas and Electric Company utilizing a saline porous rock formation in California. In 2022, a 60 MW project was opened using a salt cavern in Jiangsu, China, and the 100 MW Zhangjiakou project was connected to the grid in northern China.

2.6.2 Future of CAES systems

Studies are continuing to find alternative storage vessels that could be used in the future beyond the salt mines or depleted gas fields. As a solution, huge bags stored in the deep ocean will be used to store air. The pressure inside the bags will be maintained by the internal pressure of the ocean water [28]. Further, CAES can be interconnected with battery banks to enhance a hybrid renewable energy system for a clean energy transition.

2.6.3 Types of storage

There are two types of storage that are used in the world to store compressed-air, constant volume storages and constant pressure storages [28]. A specific physical boundary is used to control the volume of the storage space by the constant volume storage, while the air pressure is varying. On constant pressure storages, a constant air pressure is maintained, while the volume of the storage is varying.

2.6.4 Efficiency

CAES effectiveness is lower compared to energy storage systems like pumped hydropower plants and chemical battery solutions. When the operation of a CAES is considered, it substantially experiences compression and decompression. When the air is compressed, it gets heated. That energy is then released to the atmosphere as waste. When the air is decompressed, it cools down, which results in a lower energy output.

Table 2.3: Comparison of the advantages and disadvantages of CAES

Advantages	**Disadvantages**
Absorbs excess energy during low demand	Limited sites
Provides a better supply during peak hours	Perceived risk
Higher storage potential at low cost	High capital cost
Provides fast startup times	Technology is still developing.
Lower heat rates	Pulsed output
Requires no rare or toxic materials to operate	Energy loss during the compression and decompression
No wastage on non-renewable resources	
Do not require complicated technology.	
Easy to operate and maintain	

2.6.5 How to eliminate pulsation

The discharge air pressure fluctuations can be eliminated by connecting a vessel that accumulates compressed air delivered by the compressor (piston). Then the receiver tanks (accumulators) are used to serve as a temporary storage medium. The pulsation in the air discharge is eliminated by these accumulators. The pulsation is usually caused by a cyclic process of charging and discharging of compressors [28]. The pressure vessels can be installed either vertically or horizontally, where vertical air compressors require a minimum floor space.

2.7 Types of air turbines

There are two types of air turbines as: axial flow and radial flow. These turbines are operated with pressurized air and are generally used to drive machines or generators. The axial flow turbines are operated by the air flow blown parallel to the rotor. These are constructed in a multi-staged arrangement where each stage consists of a row of blades connected to the rotor and the stator. Then the air is blown through these stages. On radial flow turbines, the air flow is blown perpendicular to the blades connected to an impeller and discharged from the impeller center [29]. The expansion ratio of the radial turbine is about 9 to 1 in a single stage, whereas the axial turbines generally require three stages. Further, some of the advantages of radial turbines are low cost, lightweight design, durability, reparability, and efficiency at lower power ranges.

2.8 Permanent Magnet AC Generator

For the power generation of this research, a permanent magnet generator has been selected on the basis of several practical aspects, such as direct integration to the utility supply. A permanent magnet is used to create a magnetic field in the PMAC generator. In traditional generators, the excitation magnetic field is generated by a set of coils. In permanent magnet AC generators, it is generated by a permanent magnet itself, either by rotating around the rotor or with the rotor. Therefore, an external excitation is not required for permanent magnet AC generators. These generators are more efficient, compact, and lightweight. However, output can be varied with the speed and is more expensive [30].

CHAPTER 3

METHODOLOGY

In this chapter, the application of methodologies developed from the literature surveys done in Chapter 2 is explained in detail. The theoretical approaches for the selected methodologies are presented with calculations in this chapter.

3.1 Objectives

The study is focused on two main objectives: to develop an optimum wave energy extractor through an oscillating floater to produce compressed air and generate electricity.

1. Design & simulate a 1kW pilot wave energy extractor model
2. Construct the optimum design of the pilot model

3.2 Target Outcomes

The following outcomes are expected to be achieved at the end of the research.

- Wave energy conversion efficiency – 8%
- Air turbine efficiency – 50%
- Operating pressure levels – 10 bar
- Power Generation – 1kW (from 1 square meter of wave surface)

3.3 Site Selection

The initial step in developing a WEC system is selecting a site with appropriate environmental conditions. The wave patterns of the sea vary from region to region, depending on the environmental conditions. Therefore, several parameters must be considered when selecting a site. The behavior of the sea, climatic evaluation, and site-specific wave data such as wave height, speed, wavelength, water density, etc. are the main criteria that should be focused on.

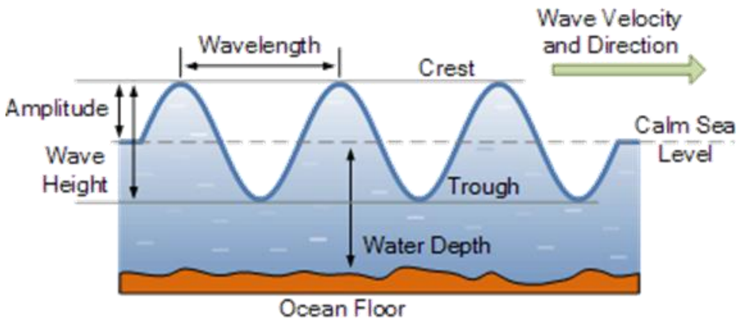

Figure 3.1: Parameters of a sea wave

As per the design, the wave energy extractor device has to be installed on the sea wave surface. It could be either onshore or offshore. The advantages and disadvantages are described in Table 3.1.

Table 3.1: Comparison of the onshore and offshore WEC systems

Location	Advantages	Disadvantages
On-shore	Close to the utility network	Lower wave power in shallow water
	Easy to maintain	Space is limited
	Damage in extreme conditions could be minimal	Visual impact
Off-shore	Higher wave power in deep water	Away from the utility network
	Expandable with enough space	Difficulty in access
	High capacity	Higher construction cost
		Higher maintenance cost

3.4 Site Selections in Sri Lanka

3.4.1 Climate seasons of Sri Lanka

The climate of Sri Lanka is dominated by the topographical features of the country and the Southwest and Northeast monsoons. Accordingly, the wind patterns are varied with directional changes. The direction of the wind is one of the causes that affect the height of the wave, other than the tidal variation. The annual climatic seasons experienced in Sri Lanka are shown in Appendix 1.

3.4.2 Selected locations for analysis

For this research, several site locations, Colombo, Weligama, and Trincomalee, in Sri Lanka, are selected for analysis of suitability of location with reference to the climatic parameters and topographical features. The annual wind patterns are referred to in the recorded Meteorological Department data, Appendix 2. The summary of the average wave height and average wind speed variation is recorded in Table 3.2.

Table 3.2: Summary of the wave height and wind speed variation

Location	Average Wave Height (m)	Maximum Wave Height (m)	Average Wind Speed (m/s)
Colombo	1.33	3.5	5.5
Weligama	1.54	3.0	5.32
Trincomalee	0.89	2.1	5.31

Based on the above analysis, Weligama is the most suitable area for wave energy extraction. However, note that the site parameters for the design calculation are referred to according to the values of Trincomalee. The selection is based on the basis of easiness in accessibility to marine environmental parameters.

3.5 Theoretical Calculations

3.5.1 Wave power calculation

To achieve the main objective of this research, energy has to be extracted from sea waves. Therefore, a surface area of 1 m^2 is used to extract wave energy. The wave power depends on the wave height, wave period, and water density. This is also known as the energy flux per unit width of a wave (power per meter of wave front). It is given by Equation 1.

$$P = \frac{\rho g^2 H^2 T}{64\pi} \qquad \text{... Equation [1]}$$

P – Wave power per meter of wave front (kW/m)

P – Sea water density (~1025 kg/m^3)

g – Gravitational acceleration (9.81 m/s^2)

H – Wave height (m)

T – Wave period (s)

Based on the research parameters, the maximum wave height at Trincomalee is 2.1 m.

The wave period is 10 s.

Hence, the power per meter of wave front is,

$$P = \frac{1025 \times 9.81^2 \times 2.1^2 \times 10}{64\pi} = 21.6\ kW/m$$

To determine the wave power per square meter, the wavelength (λ) has to be considered.

Assuming a wavelength of 15 m, the wave power per square meter of wave front is,

$$\frac{P}{\lambda} = \frac{21.6}{15} = 1.44\ kW/m^2$$

Therefore, for a 1 m^2 area of sea wave surface, there is a wave power capacity of 1.44 kW/m^2 to a wave height of 2.1 m, wave period of 10 s, and wave front of 15 m. Since the availability of this wave power capacity was the basis for selecting the generation of 1 kW from the sea surface area of 1 $m^{2,}$ as the main objective of the research.

3.5.2 Wave energy

When it is considered that the energy flow of the complete system, the initial energy for the whole process, is generated from the wave energy. Assuming the existing wave patterns are periodic, the total energy stored in the wave per square meter is,

$$E = \frac{\rho g H^2}{8} \qquad \text{... Equation [4]}$$

E – Periodic wave energy (J/m^2)

P – Sea water density (~1025 kg/m^3)

g – Gravitational acceleration (9.81 m/s^2)

H – Wave height (m)

When this relates to the maximum wave conditions at Trincomalee, H = 2.1 m,

$$E_{2.1} = \frac{1025 \times 9.81 \times 2.1^2}{8} = 5407.7\, J/m^2$$

Therefore, 5407.7 J of wave energy is available from 1 m^2 of wave surface of wave height 2.1 m (maximum).

Following Equation 2, an average wave height at Trincomalee is 1.6 m,

$$E_{1.6} = 3139.2\ J/m^2$$

Following Equation 2, for the measured wave height at Trincomalee, 0.625 m, the available energy is,

$$E_{0.625} = 479\, J/m^2$$

Note that wave height varies with the environmental and weather conditions, such as the effect of low tide and high tide, speed of the wind, period of the year, etc. The measured wave height at Trincomalee corresponded to the date of 28.08.2022.

3.5.3 Selection of conversion method

With reference to Section 2.2 of Chapter 2, the floating in-air converter type [22] is selected for the design of the oscillating system. The selection is based on advantages such as a simple structure, ease of maintenance, and no underwater operation.

3.6 Floater designing

The fundamental theory for the design calculation approach is based on the upthrust force exerted on a floating object by the sea wave surface.

Upthrust = Apparent loss of weight of object = Weight in air - Weight in liquid

$$\boldsymbol{F_a = -\rho g V} \qquad \text{... Equation [5]}$$

Density of sea water = 1026 kg/m^3

Gravitational acceleration = 9.81 m/s^2

Let dimensions of the floater to be;

Length (L) = 1 m

Width (W) = 0.8 m

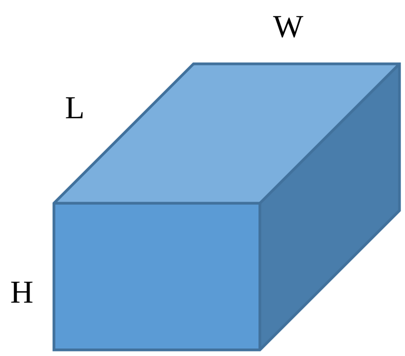

Figure 3.2: Floater dimensions

Height (H) (to be submerged) = 0.621m

Then;

$F = 1026\ kg/m^3 \times 9.81\ m/s^2 \times 1\ m \times 0.8\ m \times 0.621\ m$

$F = \underline{\underline{5000.3\ N}}$

3.7 Arm designing

The upthrust exerted on the floater is transferred to an arm through a connecting rod. The arm is acting as a lever where the fulcrum rests at a point. The moment or the relation between the ratios of the distances d1:d2 is used to determine the expected load (R) at the end B. Using this ratio, the force at the end B can be varied accordingly. As it is required to increase the force at B, the distance between A and the fulcrum has to be greater than the distance between the fulcrum and B, as these are inversely proportional, referring to Equation 5.

Considering class I lever type,

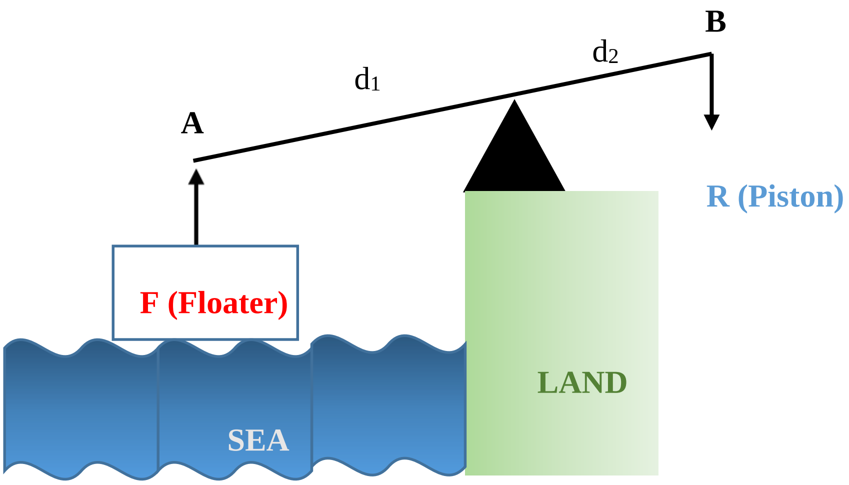

Figure 3.3: Forces acting on the lever

The moment of action on both sides of the lever is equal.

Therefore;

$$F \times d_1 = R \times d_2 \qquad \text{... Equation [6]}$$

Let;

d_1 – Distance from floater end to fulcrum = 2m

d_2 – Distance from piston end to fulcrum = 1m

5000N × 2m = 1m × R

R = 10000 N

3.7.1 Pressure Calculations

As per the design, the air has to be compressed into an accumulator and will be discharged to generate electricity. Thus, the force R created at B is transferred to a piston to compress air into the accumulator. From this section, the pressure generated at the piston end is calculated.

Pressure on Floater;

$$Pressure\ (P) = \frac{Force\ (F)}{Area\ (A)} \quad \text{... } Equation\ [7]$$

$$Pressure\ (P1) = \frac{5000\ N}{1\ m * 0.8\ m}$$

$$Pressure\ (P1) = 6250\ N/m^2$$

$1\ N/m^2 = 1$ Pascal = 0.00001 bar

Hence, pressure at the Piston end,

$$Pressure\ (P2) = \frac{10000N}{A1}$$

If the area of the piston is 0.01 m^2, the pressure at the piston head will be,

$$Pressure\ (P2) = \frac{10000\ N}{0.01\ m^2}$$

$$Pressure\ (P2) = 1000000\ N/m^2$$

i.e.,

$$Pressure\ (P2) = 10\ bar$$

Hence, a pressure of 10 bar can be absorbed at the piston head.

3.8 Piston cylinder design

With reference to the above calculation, the pressure at the piston end is 10 bar. Accordingly, the surface area is $0.01\ m^2$. Therefore, the diameter can be calculated as follows.

Area of the cylinder;

$$A = \pi r^2 \quad \text{... Equation [8]}$$

The diameter (d) can be derived as,

$$d = 2 \times \sqrt{\frac{A}{\pi}} \quad \text{... Equation [9]}$$

The diameter (d) of the cylinder is 11.3 cm.

3.9 Displacement calculation

To calculate the displacement of the piston movement, the wave height variation has to be considered. From the analysis of environmental factors, Trincomalee has an average tide height of 0.625 m and 27.4 km/h for the two months of July and August. The variation of wave height is clearly shown in Figure 3.4 and Figure 3.5.

Figure 3.4: Sea level at low tide

Figure 3.5: Sea level at high tide

Therefore, the rise in water level was taken as 0.625 m for calculations.

Now let's calculate the displacement at the piston end.

$$S = r\theta \quad \text{... Equation [10]}$$

S – Arc length

r – Radius

θ – Angular displacement

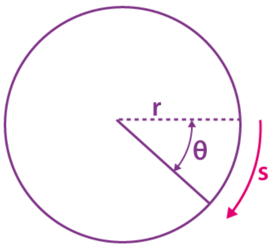

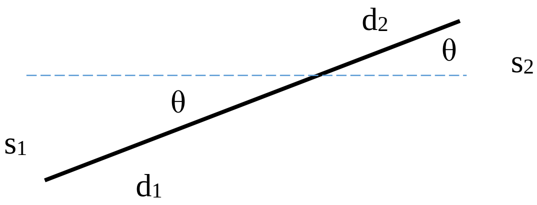

Since, θ is equal at the fulcrum,

$$\frac{s_1}{d_1} = \frac{s_2}{d_2} \qquad \text{... Equation [11]}$$

Let;

$s_1 = 0.625$ m, $d_1 = 2$ m, $d_2 = 1$ m,

$$s_2 = \frac{0.625\ m * 1\ m}{2\ m}$$

$$s_2 = 0.3125\ m$$

$$s_2 = 31.25\ cm$$

That means the displacement on the piston cylinder should be 31.25 cm to gain 10 bar out of a 0.8 m^2 surface area floater.

3.10 Design of a receiver tank

The compressed air from the piston is stored in a receiver tank (accumulator). Hence, the capacity of the receiver tank has to be determined by the following receiver tank sizing formula [31].

$$\boldsymbol{V = \frac{Q \times P_a}{P_1 + P_a}} \qquad \text{... Equation [12]}$$

V - Receiver size in cubed feet (m^3)

P_a - Standard atmospheric pressure (kPa)

Q - Compressor output (m^3/min)

P_1 - Compressed pressure (kPa)

PSIA - PSI Absolute

Absolute pressure is measured relative to a full vacuum. The pressure of a vessel completely void of any air molecules would be 0 PSIA, while average atmospheric surface pressure (at sea level) is roughly 14.7 PSIA.

PSIG -PSI Gauge

Gauge pressure is measured relative to ambient atmospheric pressure. A vessel completely void of any air molecules (at sea level) would be roughly -14.7 PSIG, and ambient air pressure is always measured as 0 PSIG.

Design of a Receiver Tank using Equation 12.

$$\boldsymbol{V = \frac{Q \times P_a}{P_1 + P_a}}$$

Assumption: Flow rate from piston (Q) = 10 bar/min

10 bar/min = 1.19 m^3/min

Pa = 14.7 psia * 6.89 = 101.283kPa

1 bar = 14.503 psi = 100 kPa

P1 = (10*100kPa) = 1000 kPa

V = (Q x Pa) / (P1 + Pa)

V = 0.091 m^3

1 m^3 = 1000 Liters

ie,

Volume = 91 Liters

3.11 Air storing mechanism

The compressed air is stored in an accumulator sized as in the above section. Then the stored air is released as required to a turbine for electricity generation. However, if there is only a single accumulator, the system output is not continued. There are drops between two cycles. Therefore, the output from the generator is also not uniform. To mitigate that, a series of accumulators connected in parallel can be used. Thus, the output will be smooth. For this development, two accumulators are used to demonstrate a uniform output. Each accumulator has an inlet and an outlet. The operation is scheduled as follows: when the inlet of Accumulator 1 and the outlet of Accumulator 2 are opened, Accumulator 1 gets filled and Accumulator 2 is discharged. At the same time, the outlet of the Accumulator 1 and the inlet of the Accumulator 2 are closed. This pattern is continuing throughout in a cyclic movement. The matrix operation is further detailed in Table 3.3 and illustrated in Figure 3.6.

Table 3.3: Truth table for matrix operation

Accumulator 1		Accumulator 2		Output
In1	Out1	In2	Out2	
1	1	1	1	0
1	1	1	0	0
1	1	0	1	0
1	1	0	0	0
1	0	1	1	0
1	0	1	0	0
1	0	0	1	1
1	0	0	0	0
0	1	1	1	0
0	1	1	0	1
0	1	0	1	0
0	1	0	0	0
0	0	1	1	0
0	0	1	0	0
0	0	0	1	0
0	0	0	0	0

The sequence controlling of the valves is automated by the Arduino Uno micro-controller. With reference to the truth table, the inputs and outputs are defined based on time controlling. Advance controlling can be set up by using pressure sensors. Solenoid pneumatic valves have been used for valve control.

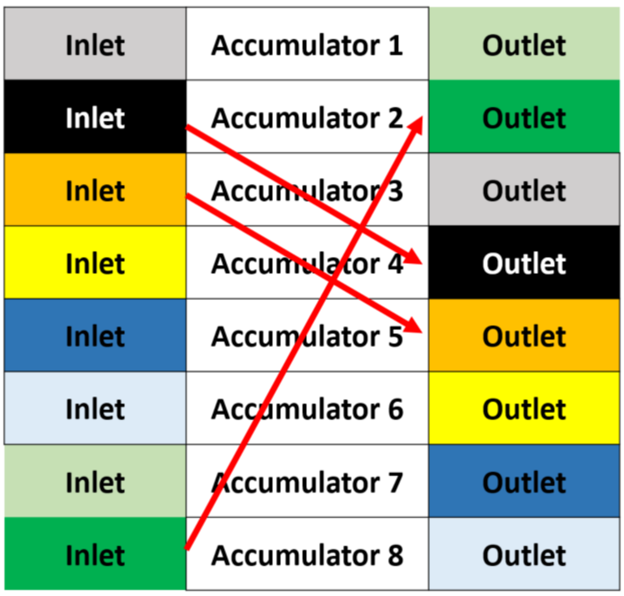

Figure 3.6: Valve Operation for a Grid of Accumulators

CHAPTER 4

SIMULATIONS

The theoretical calculations assessed in Chapter 3 are simulated in this chapter. With the non-existence of a single platform to simulate the complete system from energy extraction to electricity generation, the simulations have been performed on a stage basis with the available resources. The CAD and CFD models are used for this research, partially. The sub-sections, such as energy extractor, wave patterns, framework, and valve operation, were simulated using CAD, CFD, and micro-controlling. Though the rest of the system was also tried to be simulated with existing CFD simulation platforms, it was not succeeded with the available software and hardware resources. Mainly, the system was modelled for the following sub-sections,

1. Mechanical Energy from Sea Wave (Floater)
2. Mechanical Energy to Force Amplification (Fulcrum)
3. Mechanical Energy to Hydraulic Energy (Piston Compression)
4. Compressed Air to Kinetic Energy (Nozzle)
5. Kinetic Energy to Mechanical Energy (Pelton Wheel)
6. Mechanical Energy to Electrical Energy (Generator)

For sub-sections 1 and 2, the energy extraction model was implemented as per the same simulated criteria based on the design calculations and was simulated using ANSYS after a series of test trials with SimFlow, COMSOL, and MATLAB. The valve sequence operation of the compressed air handling system was modelled from an ARDUINO microcontroller. However, the simulations for the sub-sections 3 and 4, air compression and air storage, had to be changed due to several practical issues. Comparatively, it took a considerable research period to resolve those issues, since this was conducted as a conceptual study. Those practical issues were mainly due to the availability of resources for simulations. Also, the cost of materials impacts the variation. Since this project was self-funded, the financial affordability affected the outcome. Therefore, some of the design parameters had to be adjusted with the availability of resources and materials.

4.1 Computer-Aided Drawings (CAD)

To select the best fit shape out of the following shapes, AutoCAD 3D modelling and SolidWorks 3D modelling applications are used. Figure 4.1 shows the modelled shapes.

- Box shape
- Boat shape
- Cylinder shape
- Anchor shape

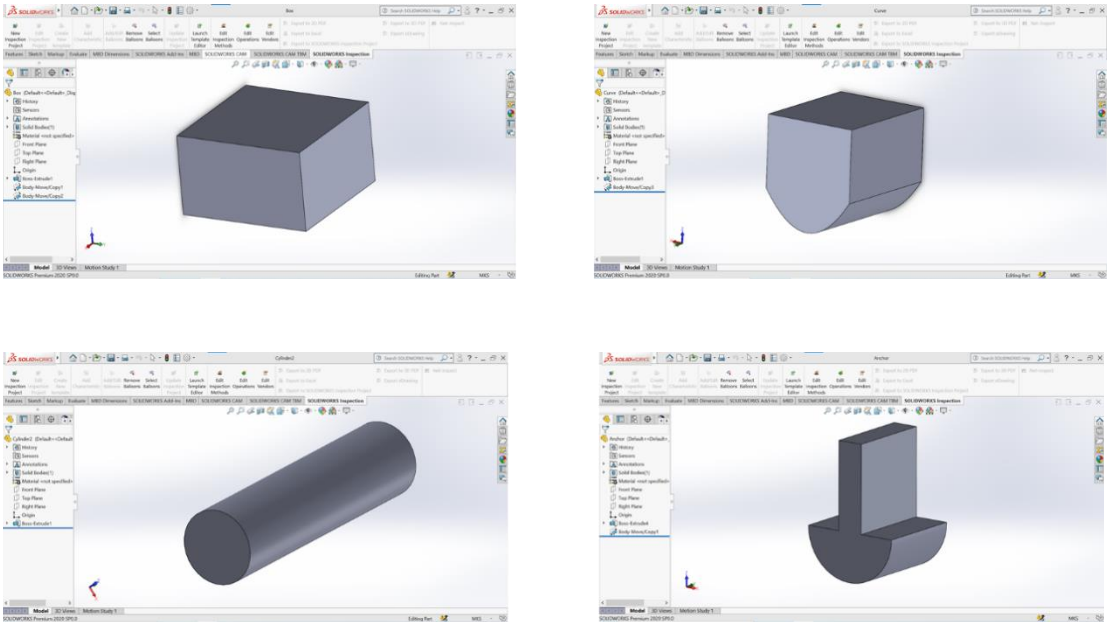

Figure 4.1: CAD modelled floater shapes

4.2 Computational Fluid Dynamics (CFD)

Use numerical analysis and data structures to analyze and solve problems that involve fluid flows.

4.2.1 Floater design

Ansys AQWA WAVE is used to simulate the floater shape design. The CAD-modelled elements are used under defined parameters for advanced CFD calculations to simulate the required movements of sea waves. The referred densities, wave heights, and wave frequencies are used for simulations.

4.2.2 Design procedures

- Defining the geometry and physical bounds using computer-aided design (CAD)
- Meshing the volume occupied by the fluid into discrete cells
- Defining the physical modelling
- Defining the boundary conditions
- Simulation
- Using a postprocessor for the analysis and visualization of the resulting solution

The simulations for the selection of the best-fit floater design were done on two approaches. The floater density and surface area of contact were kept constant throughout the simulation. While for Case 1, the weight of the floater was varied, and for Case 2, the weight of the floater was kept constant. The density of seawater was considered as 1025 kg/m^3, the surface area of water contact was considered as 1 m^2, the wave frequency was approximated as 5 rad/s, and the wave amplitude was taken as 1 m. For the environmental factors, the average wave height and the average wind speed at Trincomalee were considered as 0.89 m and 5.31 m/s, respectively. The floaters were assumed to be hollow for the simulations.

The Ansys internal environment parameters were set as such: Water Depth = 3 m, Water Density = 1025 kg/m^3, Gravity = 9.80665 m/s^2, Water Size X = 10 m, and Water Size Y = 3 m.

4.2.3 Floater design – Case 1

Using Ansys, the selected shapes are simulated to find the most efficient shape as per the given parameters for case 1. The floater height variation with respect to the wave simulation is monitored from this simulation. The snaps from the output visualization for each selected shape are given below.

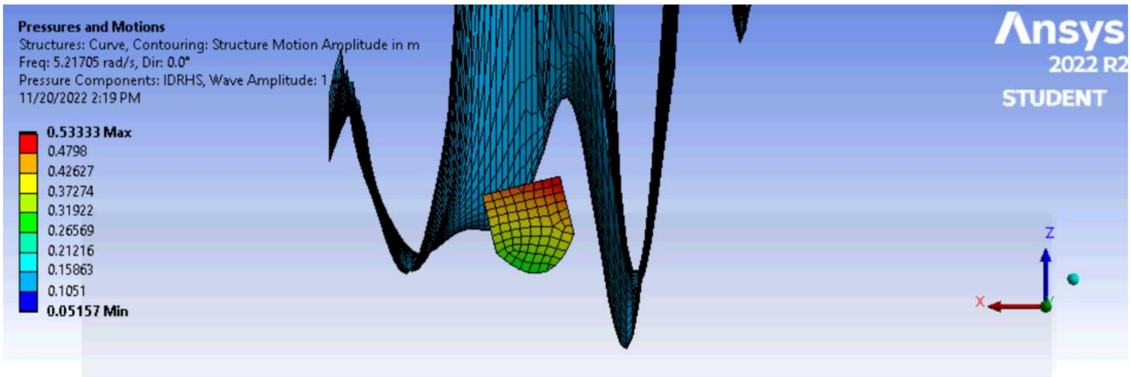

Figure 4.2: Ansys simulation of boat shape

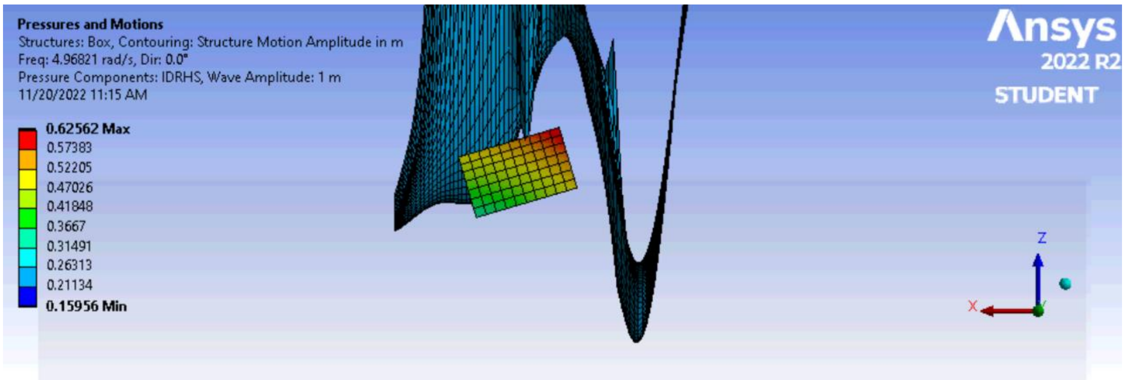

Figure 4.3: Ansys simulation of box shape

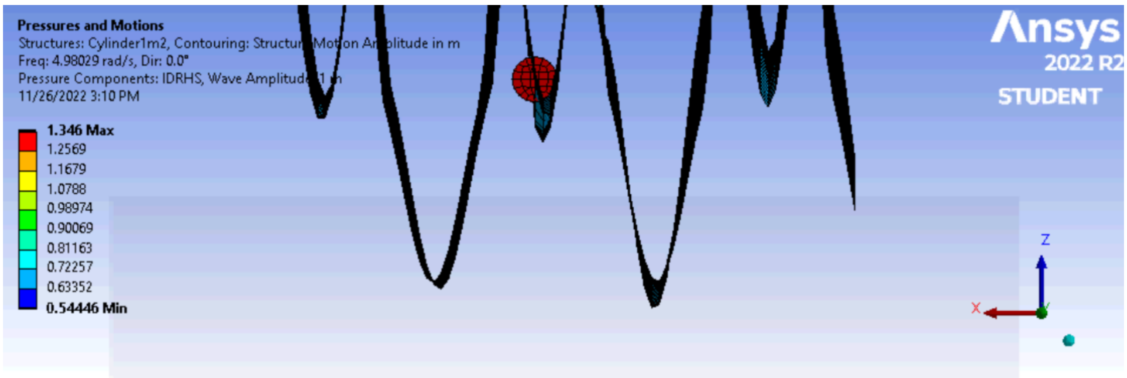

Figure 4.4: Ansys simulation of cylinder shape

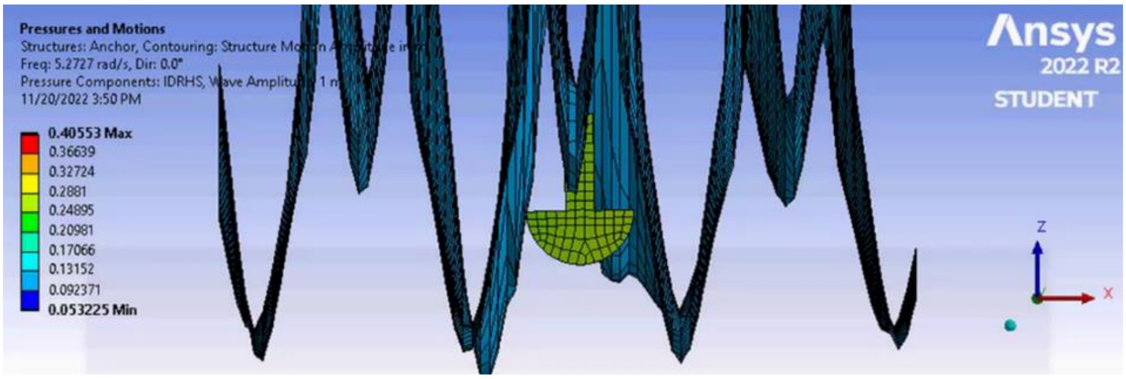

Figure 4.5: Ansys simulation of anchor shape

4.2.4 Floater design – Case 2

Using Ansys, the following shapes are simulated to find the most efficient shape as per the given parameters, keeping the weight of the object constant for case 2.

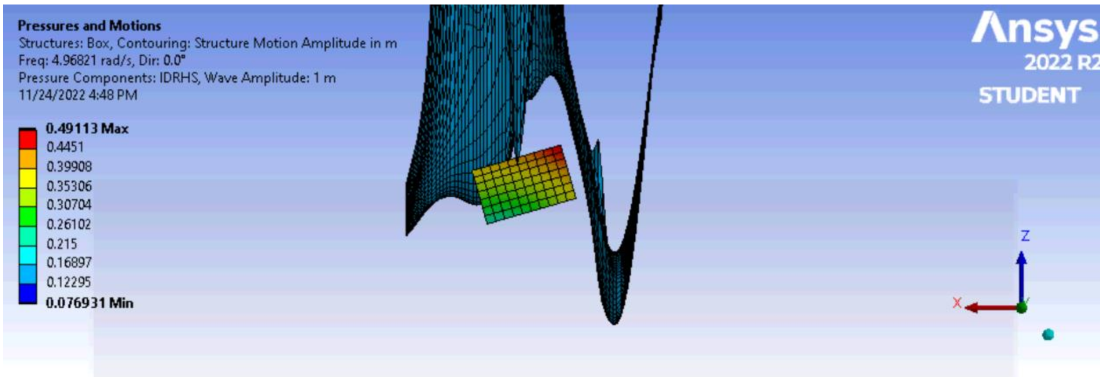

Figure 4.6: Ansys simulation of box shape

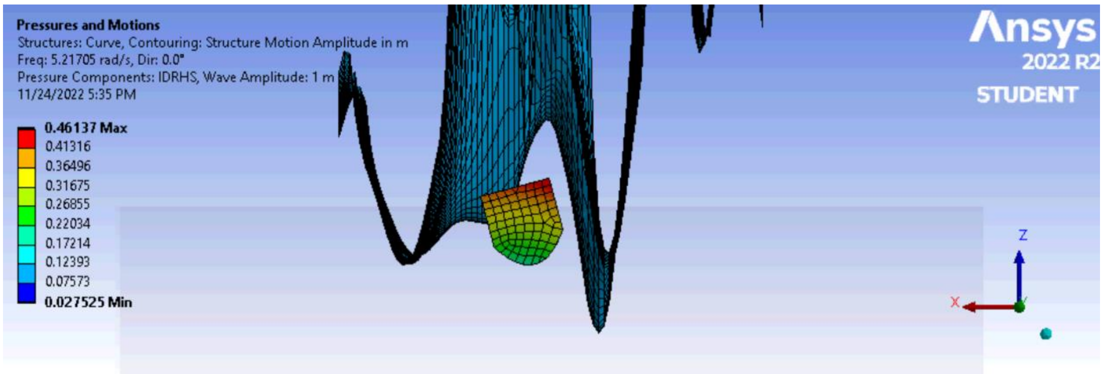

Figure 4.7: Ansys simulation of boat shape

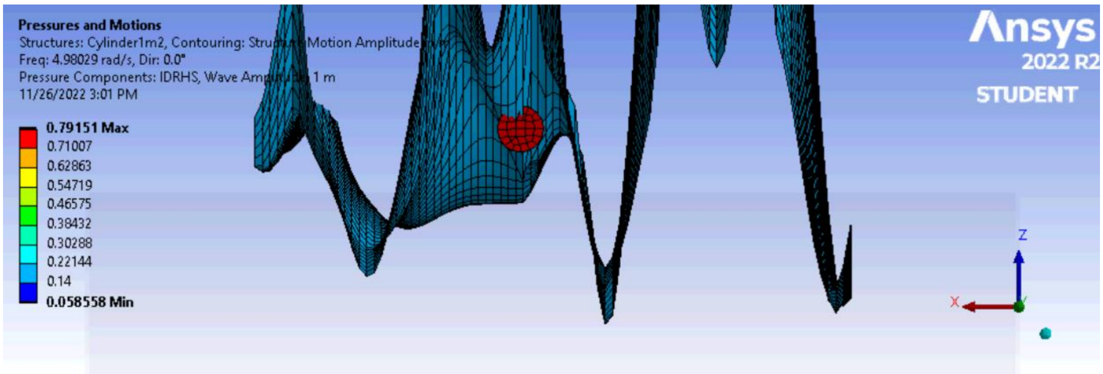

Figure 4.8: Ansys simulation of cylinder shape

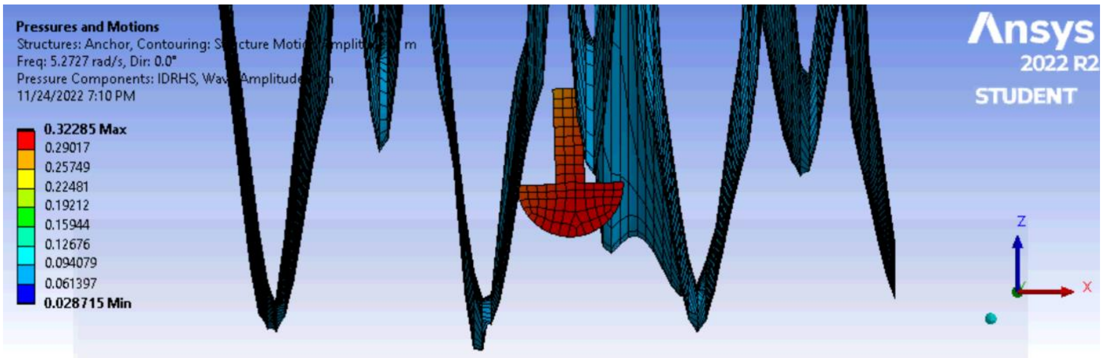

Figure 4.9: Ansys simulation of anchor shape

4.2.5 Simulation summary

The outcomes from the simulations in Section 4.2.3 and Section 4.2.4 are tabulated separately in Table 4.1 and Table 4.2. From the extracted results, the wave displacement differences are presented in Table 4.3.

Table 4.1: Simulation summary for Case 1

Object	Length (m)	Width (m)	Height (m)	Surface Area (m2)	Weight (kg)	Density (kg/m3)	Wave Freq. (rad/s)	Wave Amplitude (m)	Max Displacement (m)	Min Displacement (m)	Difference (m)
Box	1.00	1.00	0.60	1.00	307.50	512.50	4.96821	1.00	0.62500	0.15900	0.46600
Boat	1.00	0.80	0.90	0.80	328.00	512.50	5.21705	1.00	0.53333	0.05157	0.48176
Cylinder	2.00	0.5	1.00	1.00	201.23	512.50	4.98029	1.00	1.34600	0.54446	0.80154
Anchor	1.12	1.00	1.56	1.12	404.12	512.50	5.2727	1.00	0.40553	0.05323	0.35231

Table 4.2: Simulation summary for Case 2

Shape	Length (m)	Width (m)	Height (m)	Surface Area (m2)	Weight (kg)	Density (kg/m3)	Wave Freq. (rad/s)	Wave Amplitude (m)	Max Displacement (m)	Min Displacement (m)	Difference (m)
Box	1.00	1.00	0.60	1.00	500.00	512.50	4.96821	1.00	0.49113	0.076931	0.414199
Boat	1.00	0.80	0.90	0.80	500.00	512.50	5.21705	1.00	0.46137	0.027525	0.433845
Cylinder	2.00	0.50	1.00	1.00	500.00	512.50	4.98029	1.00	0.79151	0.058558	0.732952
Anchor	1.12	1.00	1.56	1.12	500.00	512.50	5.2727	1.00	0.32285	0.028715	0.294135

Table 4.3: Wave displacement differences for the best-fit shape

Shape	Case 1	Case 2
Cylinder	0.801m	0.732m
Boat	0.481m	0.434m
Box	0.466m	0.414m
Anchor	0.352m	0.294m

Out of the two cases, the cylinder shape is more suitable for the floater to have a maximum displacement.

4.3 Air storing mechanism

As mentioned in Section 3.11 of Chapter 3, the pneumatic control is operated as shown in Figure 4.10. The sequence operation of valves is simulated using an Arduino Uno micro-controller.

4.3.1 Schematic layout - Pneumatic

The circuit arrangement of the pneumatic controller is shown in Figure 4.10. The code of the control is annexed to Appendix 3.

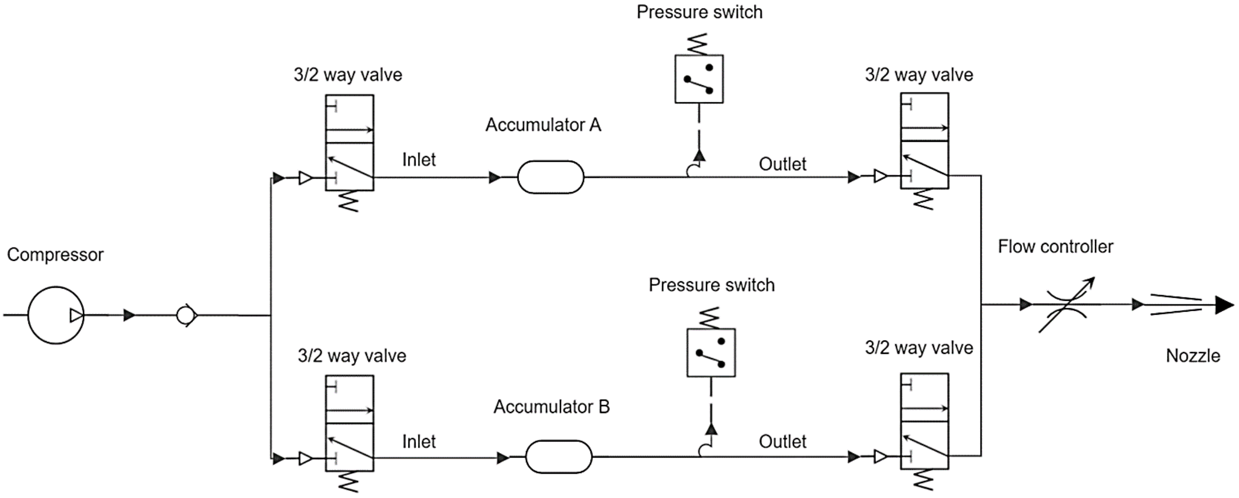

Figure 4.10: Schematic diagram of pneumatic circuit

4.3.2 Sequence controlling - Arduino

The solenoid valves are operated from a 230V AC supply. Therefore, four relays are used to control the solenoid valves. The specific valve is operated from the controller signal output. The wiring diagram is shown in Figure 4.11.

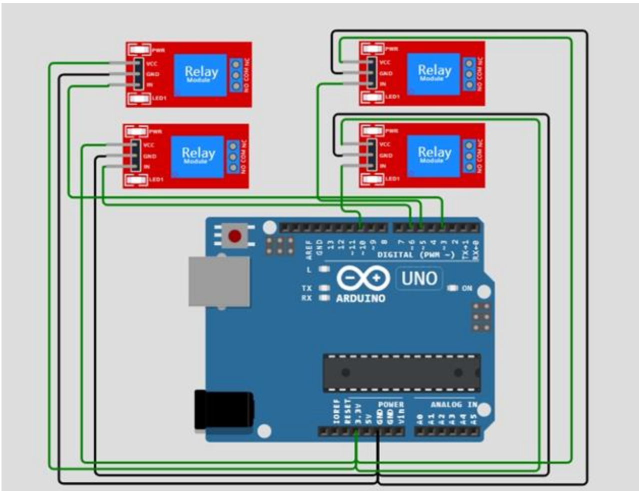

Figure 4.11: Wiring diagram of Arduino circuit

4.4 3D modelling of the system

The complete system is modelled through AutoCAD as per design parameters. Hence, the pilot model is fabricated accordingly.

4.4.1 AutoCAD model design

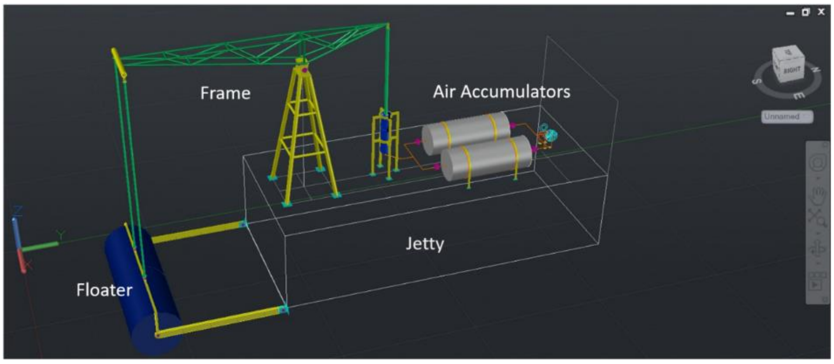

Figure 4.12: Isometric view of the design

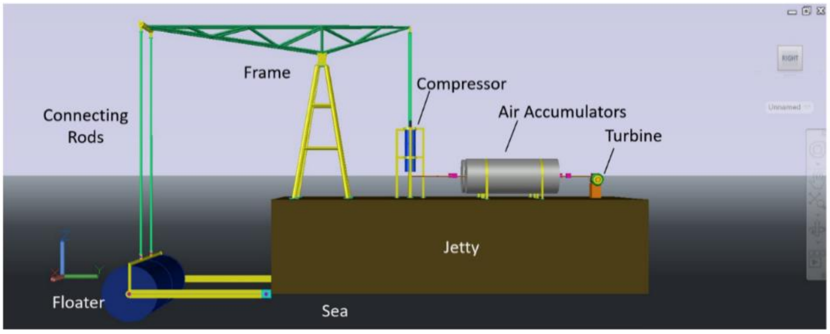

Figure 4.13: Side elevation

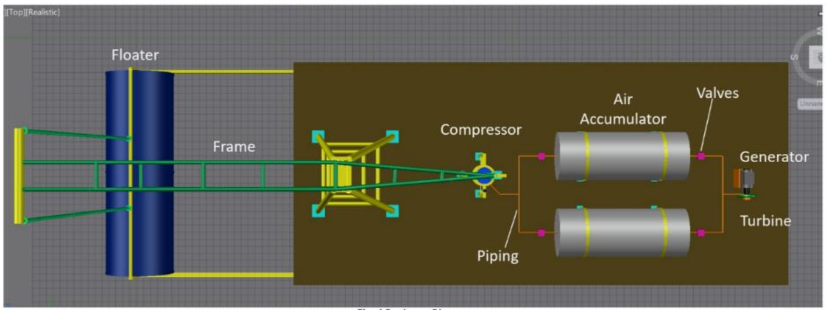

Figure 4.14: Plan view

4.4.2 Floater design details

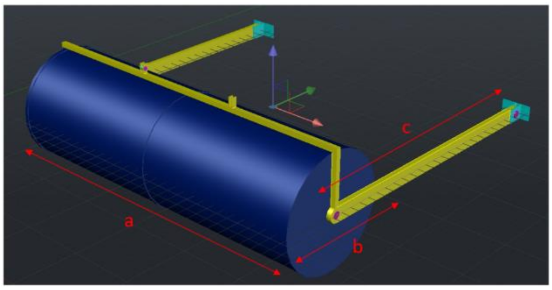

Figure 4.15: Floater design

Table 4.4: Floater design details

Section	Description	Dimension
a	Floater Length	1800 mm
b	Floater Diameter	600 mm
c	Supporting Arm	1500 mm

4.4.3 Jetty design details

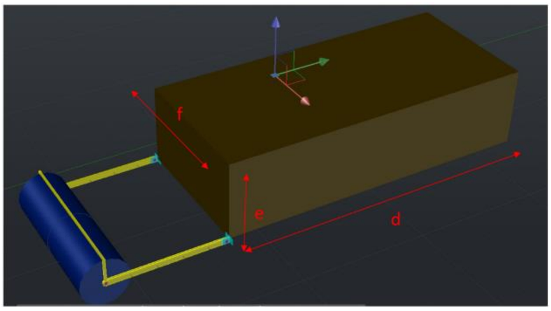

Figure 4.16: Jetty design

Table 4.5: Jetty design details

Section	Description	Dimension
d	Jetty Length	4000 mm
e	Jetty Height	1000 mm
f	Jetty Width	1800 mm

4.4.4 Main structure design details

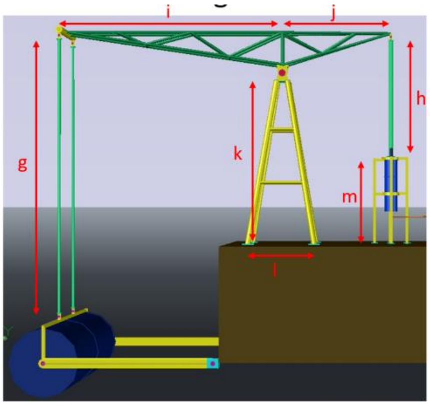

Figure 4.17: Main structure design

Table 4.6: Main structure design details

Section	Description	Dimension
g	Floater Connecting Rod	2480 mm
h	Piston Connecting Rod	1420 mm
i	Jib Length	2000 mm
j	Jib Length	1000 mm
k	Structure Main Column Height	1500 mm
l	Structure Main Column Width	600mm
m	Compressor Support	800mm

4.4.5 Compressor structure design details

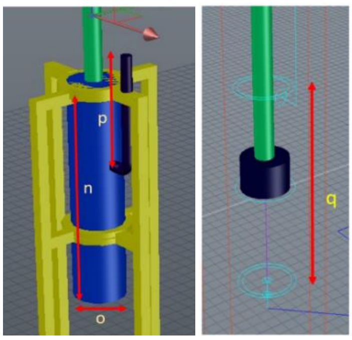

Figure 4.18: Compressor structure design

Table 4.7: Compressor structure design details

Section	Description	Dimension
n	Compressor Height	500mm
o	Compressor Diameter	120mm
p	Air Inlet	260mm
q	Piston Displacement	320mm

4.4.6 Accumulator design details

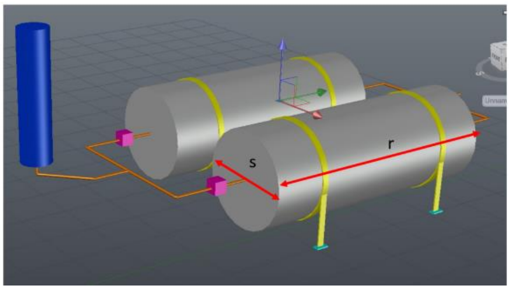

Figure 4.19: Accumulator design details

Table 4.8: Accumulator design details

Section	Description	Dimension
r	Accumulator Length	1000mm
s	Accumulator Diameter	380mm

4.5 MATLAB simulations

MATLAB is used to simulate individual sections where a single simulation platform could not process. The simulations for the wave motion are performed using MATLAB based on the wave period and design parameters as per the selected site conditions, assuming a sinusoidal wave is shown in Figure 4.20.

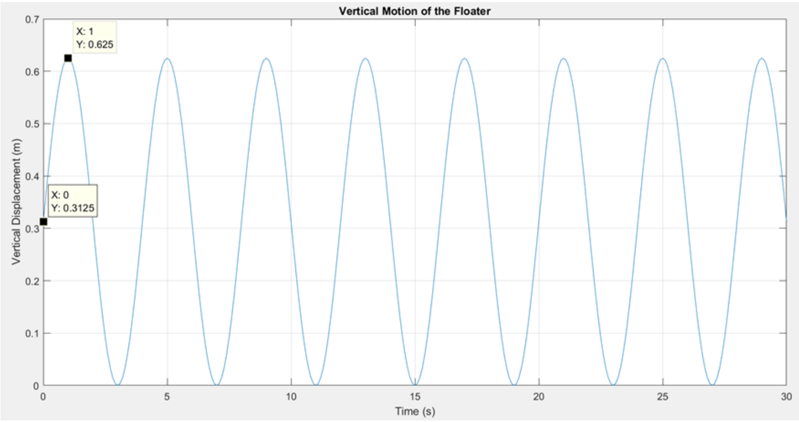

Figure 4.20: Variation of vertical displacement with time

The simulation of the displacement of the floater and the corresponding piston connected with the connection rods through the main frame is shown in Figure 4.21.

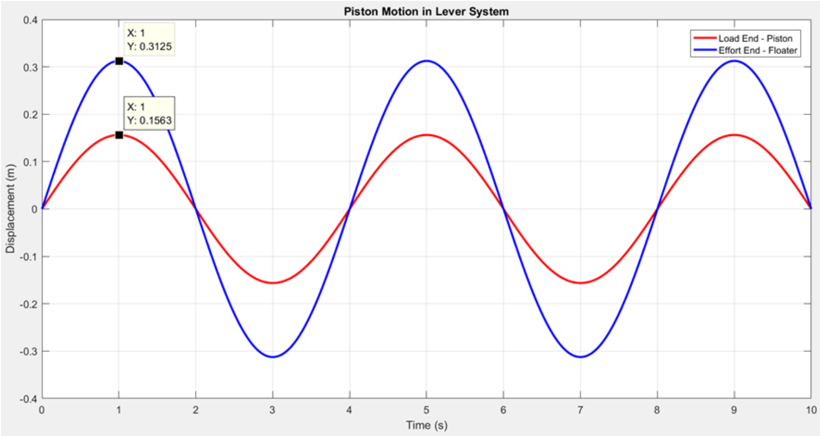

Figure 4.21: Variation of piston & floater displacement with time

The simulation of charging and discharging of the piston cylinder is shown in Figure 4.22. With reference to the design criteria, the operational pressures are between 10 bar and 1 bar. The discharging pressure is assumed to have dropped to 1 bar.

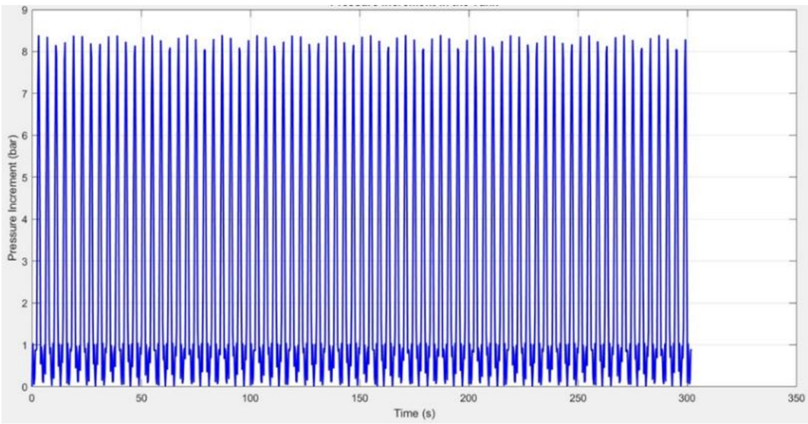

Figure 4.22: Variation of pressure increment in piston cylinder with time

The simulation of discharging pressure variation at the Pelton turbine is shown in Figure 4.23.

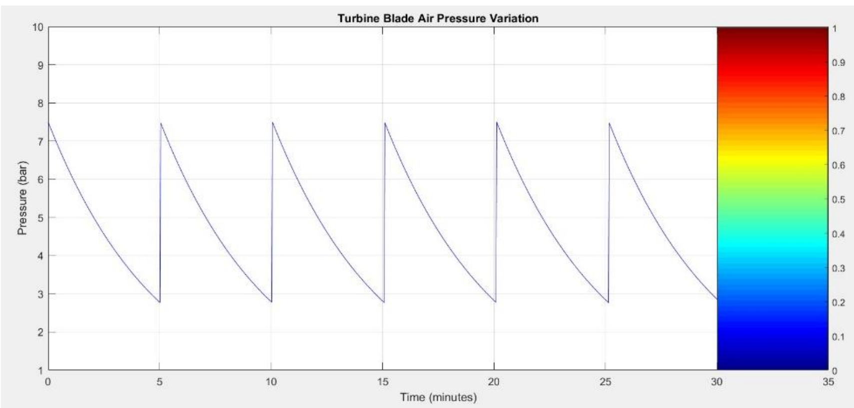

Figure 4.23: Pressure variation at Pelton wheel

CHAPTER 5

PILOT MODEL

5.1 Fabrication of the pilot model

In this chapter, the details of the actual pilot model that was fabricated according to the design parameters analyzed in Chapters 3 and 4 have been presented. The system that was designed and simulated has been tested to check the feasibility of the output of the theoretical model. However, some of the equipment has been replaced with the availability of materials at the market. Hence, there are minor deviations from the theoretical model, and these have been highlighted.

Figure 5.1: Pilot model

5.1.1 Fabrication of floater

Device Parameters

- Surface Length = 1.8m
- Diameter = 0.6m
- Surface Area = 1.08 m^2
- Supporting Arm = 1.5m

Figure 5.2: Fabricated floater

5.1.2 Piston cylinder

The piston and the cylinder, which were dimensioned from the theoretical calculations faced several complexities in fabrication. Therefore, two commercially available foot pumps with a diameter of 36 mm are used. The pressure output of these pumps is greater than the calculated values, as the surface area under the same force is small. Further, the smoothness of the operation is maintained from the in-built stock chamber.

Pressure on piston;

$$Pressure\ (P) = \frac{Force\ (F)}{Area\ (A)} \qquad \text{... Equation [7]}$$

$$Pressure\ (P1) = \frac{10000\ N}{0.002\ m^2}$$

$$Pressure\ (P1) = 4977000\ N/m^2$$

$$Pressure = 49\ bar$$

Since the rated working pressure of the pumps is 8 bar, there is no impact on the expected pressure generation as per the calculations.

5.1.3 Installation of pressure vessel

Due to the non-availability of exact-dimensioned pressure vessels as per the theoretical calculations, a locally available pressure vessel of the following parameters was used. The main drawback of this selection is the charge-discharge cycle time is higher than expected.

Device Parameters

- Accumulator Length = 500 m
- Accumulator Diameter = 230mm
- Operating Pressure = 8 bar
- Capacity = 24 L

Figure 5.3: Pressure vessel

5.1.4 Power generation mechanism

For power generation, a specific generator is used after a series of experiments with different types of generators. Since, to capture the maximum output from the pressure discharge, a Permanent Magnet 3-Phase Low RPM Generator is used. It is rated for a power output of 1000 W and a rated voltage of 12 VAC at a rated speed of 300 RPM. The type of magnet material is rare earth NdFeB. Further, the features mentioned in Table 5.1 are also concerned in the selection of this generator.

Table 5.1: Features of the permanent magnet generator

Highly efficient power generation	No gears
Stable power generation	Low starting resistance moment
Easy to operate and maintain	Good heat dissipation

5.1.5 Fabrication of air turbine

The Pelton wheel turbines are designed for converting fluid energy into rotational energy [32]. Due to its high efficiency and high torque, the Pelton wheel is used for this installation. This can also be operated at low speeds, where it is ideal for the coupled low-RPM generator.

Design Parameters

- Turbine radius = 250 mm
- No. of blades = 10
- Angle between two blades = 36°
- Height of a blade = 40 mm
- Width of a blade = 26 mm
- Depth of a blade = 14 mm

Figure 5.4: 10-blade Pelton wheel

5.2 Deviations with theoretical & actual values

Table 5.2: Deviations of the theoretical and actual values

Component	Parameter	Theoretical Value	Actual Value	No. of Units
Floater	Length	2.0 m	1.8 m	-
	Width	0.5 m	0.6 m	
Piston (Approach 2)	Diameter	113 mm	36 mm	2
	Displacement	312.5 mm	350 mm	
Accumulators	Length	1000 m	500 m	-
	Diameter	380 mm	230 mm	
Operating Pressure	Pressure	10 bar	8 bar	-

5.3 Actions to mitigate deviations – Impact on Efficiency

The following measures have been taken to mitigate the design deviations. The number of blades on the Pelton wheel is increased. The volume of accumulators can be increased to store a higher capacity of energy. The volumetric ratio of the piston and the accumulator has been maintained in a proportional relationship.

5.3.1 Modification of Air Turbine

The design parameters of the 10-blade Pelton wheel are modified as follows.

Turbine radius = 250 mm

No. of blades = 20

Angle between two blades = 18°

Height of a blade = 40 mm

Width of a blade = 26 mm

Depth of a blade = 14 mm

Figure 5.5: 20-blade Pelton wheel

After modifying the Pelton wheel by increasing the number of more blades, the performance and the efficiency are improved to harness the airflow Figure 6.8–6.12.

Table 5.3: Comparison of 10-blade and 20-blade Pelton wheel

Feature	20-Blade System	10-Blade System
Power Output	Smooth output. Ideal for consistent power applications.	Less smooth output. Higher fluctuations.
RPM Performance	Reaches higher RPM. High stability.	Reaches lower RPM. Less stability.
Efficiency	Highly responsive. Stable RPM increase.	Less responsive. Less stable RPM increase.

CHAPTER 6

ENERGY FLOW & RESULTS ANALYSIS

In this chapter, the energy flow and results analysis are discussed in detail. The energy flow diagrams in this chapter refer to the energy calculations in Section 3.5 of Chapter 3. When considering the results analysis of the research, it has been approached with two approaches: the theoretical model and the practical model. Both approaches are kept in line as much as possible to achieve the main objectives of the study. All the theoretical calculations are followed by the fundamental principles in the ideal space. However, the practical model was implemented with minor deviations from the theoretical model while maintaining the research concept intact.

6.1 Energy flow

Although wave energy is available as per Section 3.5.2 of Chapter 3, calculations for different wave heights show that the output energy is varied mainly due to several types of energy conversions and energy losses. An energy flow diagram illustrates the major variations of the energy along the system's energy conversions.

The energy conversions for this pilot project were considered at the following transitions.

1. Mechanical Energy from Sea Wave (Floater)
2. Mechanical Energy to Force Amplification (Fulcrum)
3. Mechanical Energy to Hydraulic Energy (Piston Compression)
4. Compressed Air to Kinetic Energy (Nozzle)
5. Kinetic Energy to Mechanical Energy (Pelton Wheel)
6. Mechanical Energy to Electrical Energy (Generator)

The following diagram shows the energy flow considered for the last progress review. Here, the input wave energy was considered based on upthrust. At the beginning, the calculation concept of this model was initiated with the upthrust generated by a floating load (mechanical energy is 3150 J to a force of 5000 N for 0.63 m). This was the approach that was followed throughout the design for energy calculations. The energy calculations for the whole system were continued based on the efficiencies at each energy conversion. However, based on Equation 2, the calculated value also corresponded to a wave height of 1.6 m.

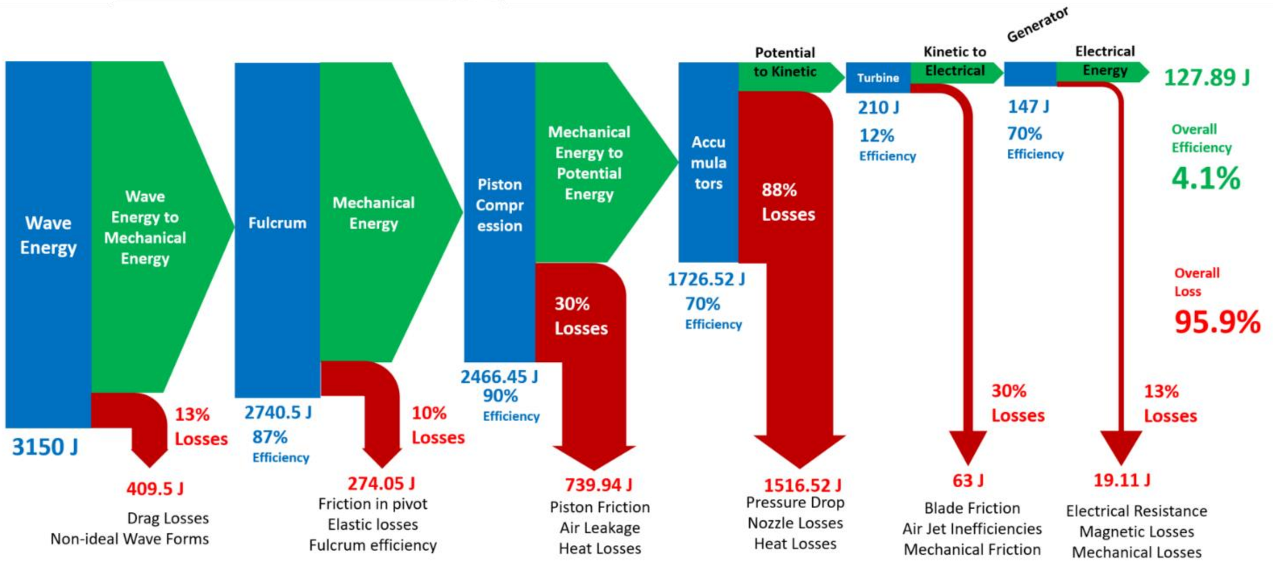

Figure 6.1: Energy flow diagram for 1.6m wave height

The following diagram shows the energy flow of the complete system based on Equation 2, considering the wave energy for a wave height of 0.625 m.

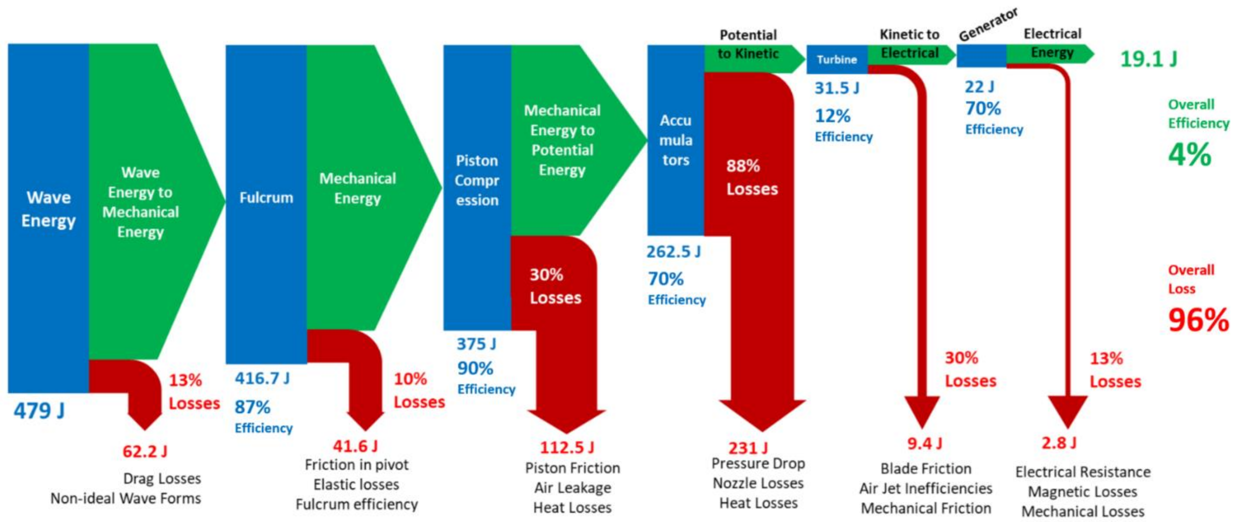

Figure 6.2: Energy flow diagram for 0.625m wave height

Considering the wave energy for a wave height of 2.1 m, the following diagram shows the energy flow of the complete system based on Equation 2.

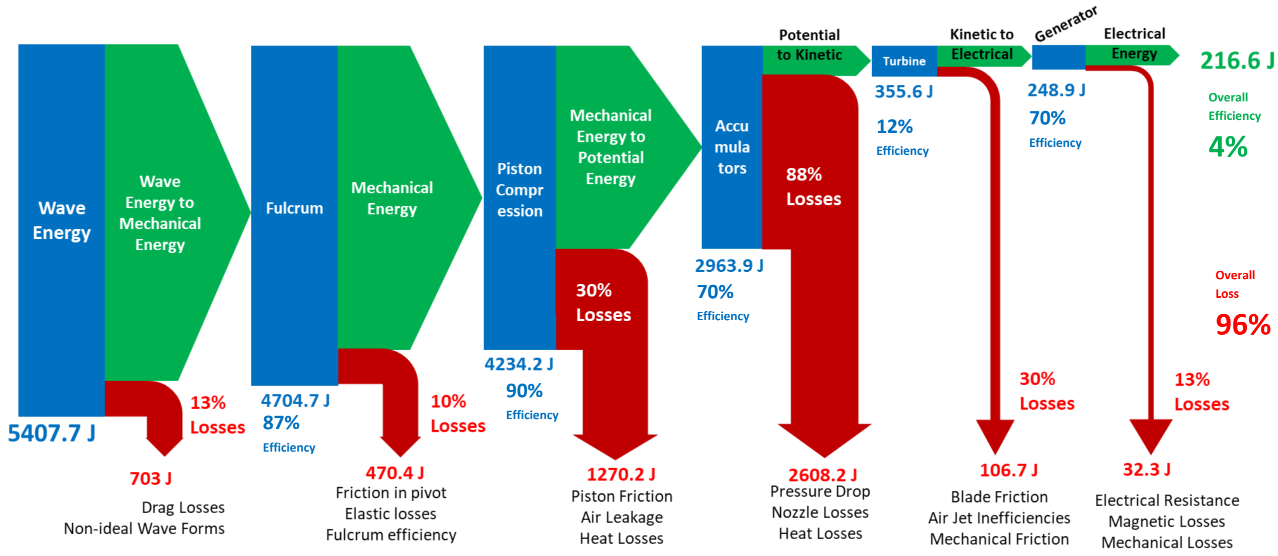

Figure 6.3: Energy flow diagram for 2.1m wave height

Based on the above energy flow diagrams, the results can be summarized as follows.

Table 6.1: Summary of efficiencies for different wave heights

Wave Height (m)	Energy In (J)	Energy Out (J)	Efficiency (η)
2.1	5407.7	216.6	4.01
1.6	3139.2	128.9	4.11
0.625	479	19.1	3.99

It seems that the overall efficiency of the proposed energy extraction method is around 4% for different wave heights.

Since the above periodic wave energy calculations were based on a time interval of 10 s, the power output of the system can be assumed as follows.

$$P = \frac{E}{t} \qquad \text{...Equation [3]}$$

E – Electrical energy output

t – Time taken for air discharge

Table 6.2: Summary of power output for different wave heights

Wave Height (m)	Energy Out (J)	Time (s)	Power (W)
2.1	216.6	10	21.7
1.6	128.89	10	12.9
0.625	19.1	10	1.9

As per the above table, the power output of 1.9 W can be extracted from a 0.625 m wave. The power output of 12.9 W & 21.7 W can be extracted from 1.6 m & 2.1 m height waves, respectively. Since there is a wave power availability of 1.44 kW per 1 m^2 of sea wave surface with a 15 m wave front, an output of 1 kW can be reached with an efficiency of 69% of the available wave power capacity. But, due to a series of energy losses at each energy conversion, the ultimate power output is only 21.7 W with reference to a 2.1 m wave height. The losses are mainly due to a large number of energy conversions in the system. So, the overall energy efficiency of this system is around 4%, which was expected to be 8% on the research target outcomes.

6.2 Calculations for models

Under this section, it explains how the theoretical model calculations and the pilot model outcomes were related to the deviations mentioned above.

6.2.1 Power output calculations - Theoretical model

For the calculations of the theoretical model, the parameters were derived from the initial design. The complete operation was separated into two main sub-sections based on energy storage and discharge. The system from energy extraction up to compression of air at accumulators (energy storage), and the system after accumulators up to power generation. These power output calculations were performed for the second subsection from air accumulators onwards.

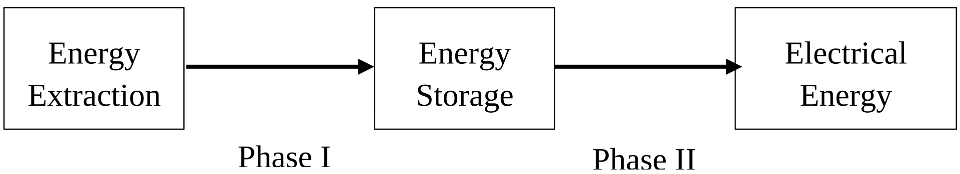

Figure 6.4: Energy flow sub sections

Energy Stored in Compressed Air (per single accumulator)

$$E_{stored} = PV \ln\left(\frac{P}{P_{atm}}\right)$$

P - Initial absolute pressure in the tank (10 bar = 10^6 Pa)

V - Volume of the tank (91 L = 0.091 m^3)

P_{atm} - Atmospheric pressure (1 bar = 10^5 Pa)

Energy stored in compressed air

Assume the pressure inside the accumulator is at 10 bar, as per the theoretical calculations.

$$E_{stored} = 10^6 \; x \; 0.091 \ln\left(\frac{10^6}{10^5}\right)$$

$$E_{stored} = 10^6 \; x \; 0.091 \; x \; 2.302$$

$$E_{stored} = 209{,}482 \; J = 209.482 \text{ kJ}$$

Electrical energy output

$$E_{electrical} = E_{stored} \; x \; \eta_{turbine} \; x \; \eta_{generator}$$

Consider,

$\eta_{turbine}$ = *70*% [25], $\eta_{generator}$ = *87*% [25]

$E_{electrical} = 209{,}482 \; x \; 0.7 \; x \; 0.87 \; J = 127{,}575$ J

The energy in 1 kWh = 3,600,000 J,

$$E_{electrical}(kWh) = \frac{E_{electrical}(J)}{3.6 \times 10^6 \; J/kWh} = \frac{127{,}575 \; J}{3.6 \times 10^6 \; J/kWh} = 0.0354 \; kWh$$

Average power output

$$P = \frac{E}{t}$$

E – Electrical energy output

t – Time taken for air discharge

For 60 s,

$$P_{electrical}(kW) = \frac{E_{electrical}(kWh)}{Time\ (h)}$$

$$= \frac{0.0354\ kWh}{0.0167\ h}$$

$$= 2.126\ kW$$

$$= 2126\ W$$

For 10 s,

$$P_{electrical} = 354.33\ W$$

From the above calculations, it is clear that the power output of the system for 60 s is 2.126 kW. However, for the linearity of the calculations from the beginning, the time period has to be in line with the wave period. Therefore, the period for the power output was concerned for 10 s, such that the power output is 354.33 W.

6.2.2 Power output calculations - Pilot model

As mentioned earlier, the pilot model was carried out under a series of practical circumstances. However, the flow of the research was maintained at its optimum level to achieve the expected outcome. Mainly, the model had to be operated at 7 bar pressure, and the volume of the pressure vessel had to be reduced up to 24 L. Based on these variations, the following calculation was done to check the conformity of the actual measurements.

Energy stored in compressed air (per single accumulator)

$$E_{stored} = PV \ln\left(\frac{P}{P_{atm}}\right)$$

P - Initial absolute pressure in the tank (7 bar = 10^6 Pa)

V - Volume of the tank (24 L = 0.024 m^3)

P_{atm} - Atmospheric pressure (1 bar = 10^5 Pa)

Energy stored in compressed air

$$E_{stored} = 7\ x\ 10^5\ x\ 0.024\ ln\left(\frac{7x10^5}{10^5}\right)$$

$$E_{stored} = 32.686\ kJ$$

Electrical energy output

$$E_{electrical} = E_{stored}\ x\ \eta_{turbine}\ x\ \eta_{generator}$$

Consider,

$\eta_{turbine}$ = *70*% [25], $\eta_{generator}$ = *87*% [25]

$E_{electrical} = 32{,}686\ \ x\ 0.7\ x\ 0.87\ J =\ 19{,}919\ J$

The energy in 1 kWh = 3,600,000 J,

$$E_{electrical}(kWh) = \frac{E_{electrical}(J)}{3.6\ \times\ 10^6\ J/kWh} = \frac{19{,}919\ J}{3.6\ \times\ 10^6\ J/kWh}$$

$$=\ 0.005528\ kWh\ = 5.52 \times 10^{-3}\ kWh$$

Average power output

$$P =\ \frac{E}{t}$$

E – Electrical energy output

t – Time taken for air discharge

For 60 s,

$$P_{electrical}(kW) = \frac{E_{electrical}(kWh)}{Time\ (h)}$$

$$= \frac{5.52 \times 10^{-3}\ kWh}{0.00167\ h}$$

$$= 0.331\ kW$$

$$= 331\ W$$

For 10 s,

$$P_{electrical} = 55.1\ W$$

6.3 Measured output – Pilot model

With reference to Chapter 5, the pilot model is developed using a 1 kW low RPM permanent magnet generator to capture the maximum energy from the available energy potential of the sea wave under 1 m^2 of surface area, since there is a wave power capacity of 1.44 kW/m^2 to a wave height of 2.1 m, wave period of 10 s, and wave front of 15 m. However, by analyzing the energy flow diagrams, it is clear that due to several energy conversions, the outcome has been reduced significantly. Hence, the model was tested under several parametric deviations to gain the optimum output as mentioned earlier. For that, different approaches were taken with the available resources. The following summary of the load tests, based on the entire load test, Appendix 5, shows the variation of output wattage with respect to the RPM of the turbine and the attached load. All these readings were taken under 7-bar pressure air discharge.

Table 6.3: Load test summary

Case	Description	Total Load (W)	Peak Power (W)	Average Power (W)
Case 1	100W Halogen Bulb x 2	200	0.120	0.116
Case 2	21W Filament Bulb x 5	105	10.200	8.697
Case 3	21W Filament Bulb x 4	84	18.684	10.396
Case 4	21W Filament Bulb x 3	63	48.521	17.814
Case 5	21W Filament Bulb x 2	42	24.640	19.943
Case 6	21W Filament Bulb x 1	21	28.059	18.392
Case 7	21W Filament Bulb x 1	21	23.835	17.932

Referring to the above results, the best performance can be identified at Case 5 with an average power output of 19.9 W. The recorded maximum volt-ampere reading was recorded at 48.5 W with Case 4.

After analyzing the above results, it was observed that the system operates efficiently under moderate loads compared to higher loads, where output power diminished significantly.

6.3.1 Efficiency of the pilot model

Average output

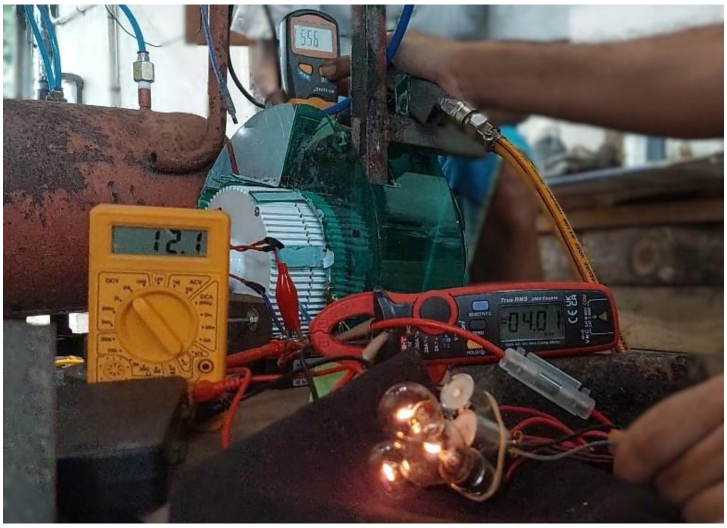

Figure 6.5: Maximum Volt Ampere Reading – 3 x 21W 12V Filament Bulbs

$$Efficiency(\eta) = \frac{Actual\ Average\ Output(W)}{Expected\ Output(W)} \times 100\%$$

$$Efficiency(\eta) = \frac{19.9\ W}{1000\ W} \times 100\% = 1.99\ \%$$

Maximum Output

$$Efficiency(\eta) = \frac{Actual\ Maximum\ Output(W)}{Expected\ Output(W)} \times 100\%$$

$$Efficiency(\eta) = \frac{48.5\ W}{1000\ W} \times 100\% = 4.85\ \%$$

From the theoretical calculations, the efficiency was calculated to be around 4% based on energy flow. Here, for the actual pilot model, the calculated efficiency from the measured parameters was 4.85% for the consideration of maximum output and 1.99% for the average output.

Further, the power output from the theoretical model and the practical model is plotted with reference to a single accumulator discharge. The spikes can be minimized by increasing the sequencing of accumulators for a continuous operation.

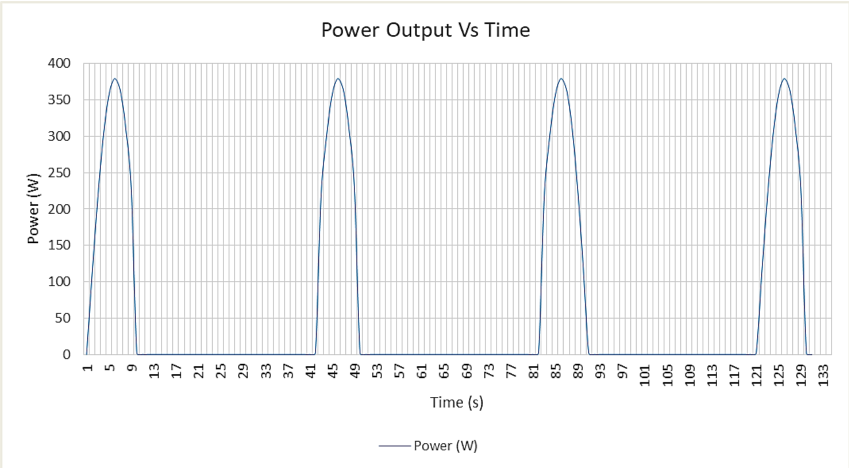

Figure 6.7: Power output of the theoretical model

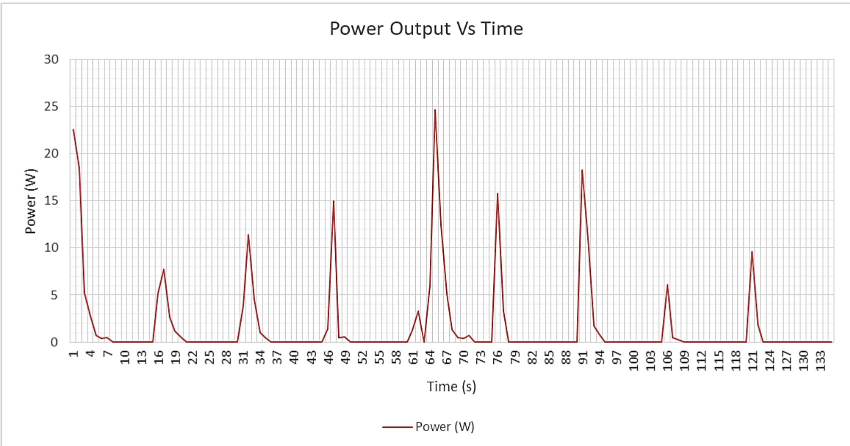

Figure 6.6: Power output of the pilot model

6.3.2 Performance variation of the Pelton wheel

As mentioned in Section 5.3.1 of Chapter 5, the number of blades on the Pelton wheel is increased to improve the performance and the efficiency of the air turbine. The variation of the voltage and the speed regarding the same air flow is shown below in the following graph. It can be identified that the performance and the smoothness of the output of the 20-blade system have been improved with reference to the 10-blade system.

Performance – Voltage Variation

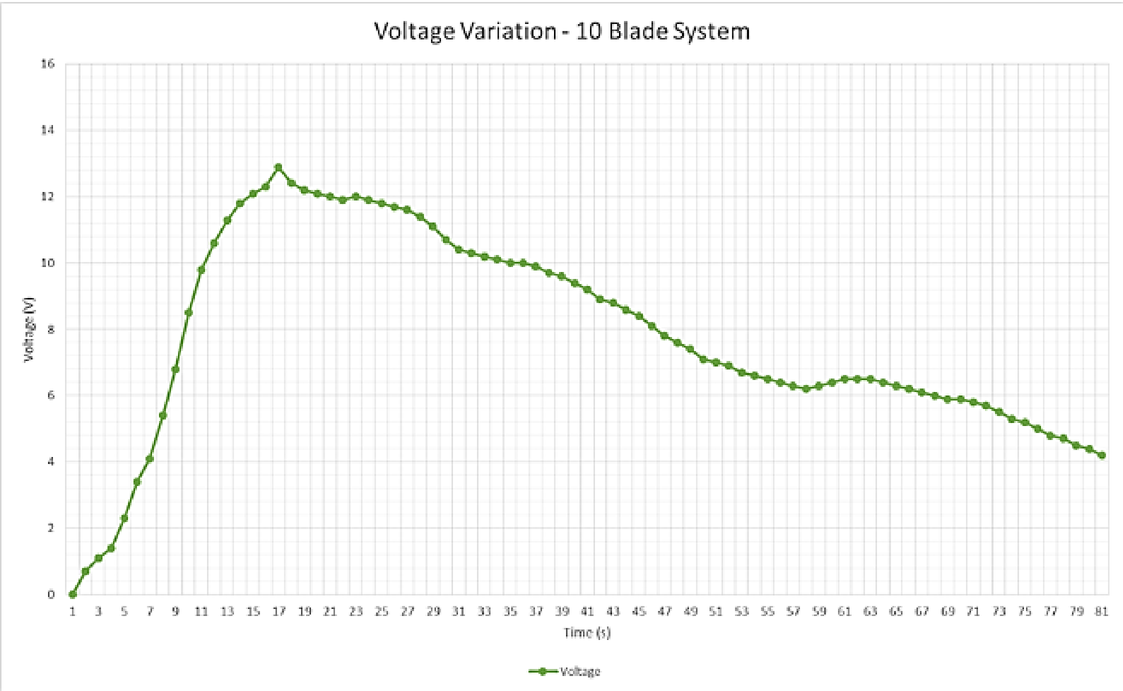

Figure 6.8: Voltage variation of 10-blade turbine

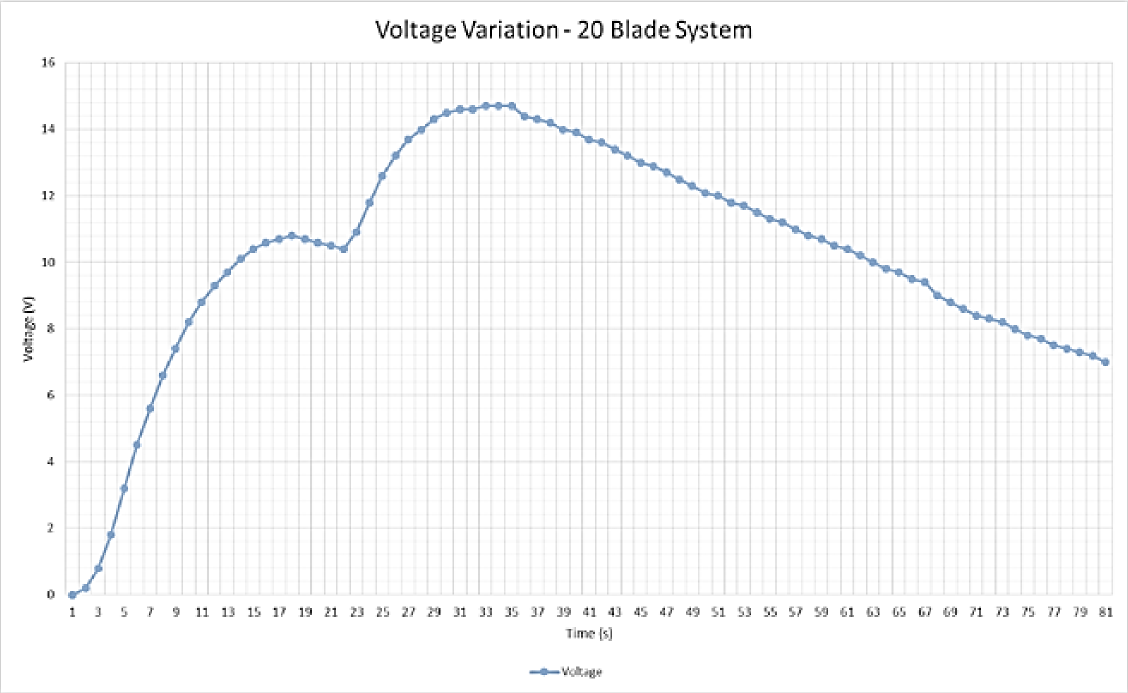

Figure 6.9: Voltage variation of 20-blade turbine

Performance – Speed Variation

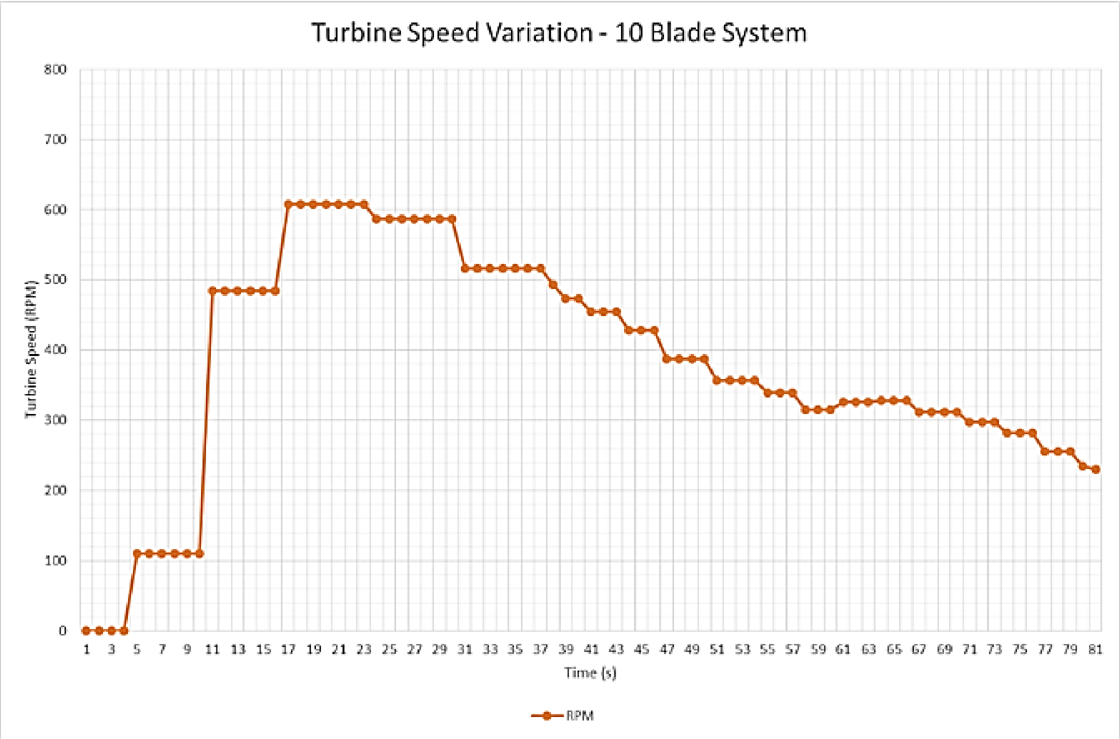

Figure 6.10: Speed variation of 10-blade turbine

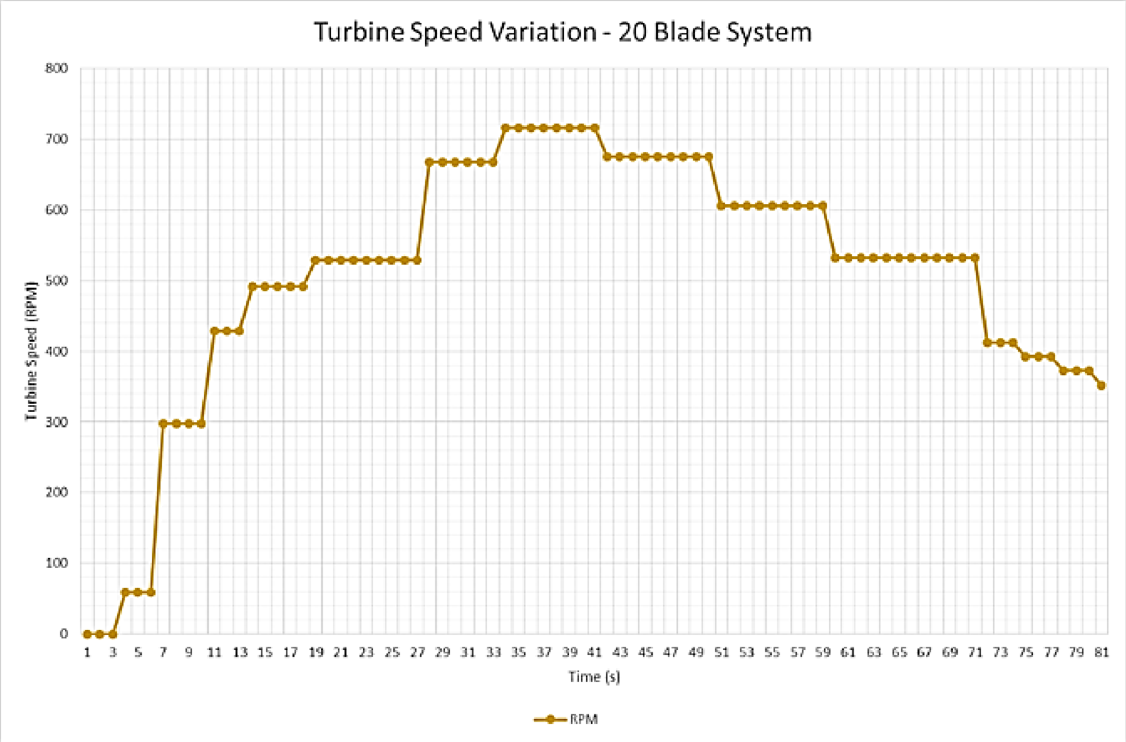

Figure 6.11: Speed variation of 20-blade turbine

CHAPTER 7

CONCLUSIONS AND RECOMMENDATIONS

7.1 Conclusions

The main objective of this research is to develop an optimum wave energy extractor through an oscillating floater to produce compressed air and generate electricity. Following this objective, a wave energy extractor model was designed and simulated to extract a capacity of 1 kW from 1 m^2 of sea wave surface based on theoretical wave energy capacities.

As described in Chapter 2, there are a number of wave energy converters operated worldwide on commercial and development scales. Of them, most existing wave energy conversion systems, including CETO, Eco Wave Power, Wave Swell Energy, and pilot-scale deployments, are facing significant limitations in commercial viability due to economic, technical, and environmental factors. Higher CAPEX on infrastructure development and higher OPEX of the structures and the storage have resulted in a significant financial burden. Grid integration and maintenance challenges, such as routine access for inspections and repairs, are especially challenging for offshore and submerged units. Scaling up to commercial-scale arrays has been complicated due to hydrodynamic interference and mooring entanglements. Due to multi-stage energy conversion losses, the typical efficiency is yielding below 25%. When considering the energy storage systems, the lifecycle of batteries is shorter compared to compressed air. The resources for the battery manufacturing process are depleting over time with the increase in demand. Also, the environmental impact of battery disposals has created a major environmental issue, claiming that CAES is a pure, clean energy storage mode. Absence of design standardization, certifications, long payback periods, and published performance data have created financial limitations for funding. Environmental limitations such as biofouling, corrosion, marine ecosystem disruption, and acoustic and visual impacts remain under-researched. Therefore, these factors highlight the need for further R&D, supportive policy frameworks, and technology standardization to make wave energy a commercially viable contributor to the renewable energy mix.

Based on the practical limitations of the existing wave energy converters and addressing the research gap related to wave energy extraction, storage, and electricity generation, this research has been conducted. Therefore, by focusing on the objectives, a pilot model was constructed to capture the maximum theoretical energy capacity with the available resources. Since this is a novel concept, no similar simulation platforms have been developed to simulate the exact system on a single simulator. However, the simulations have been operated separately for individual sub-sections to achieve the best fit outcome with the available facilities and resources. ANSYS, SimFluid, COMSOL, and MATLAB are some of the major simulation platforms used for CFDs and general simulations. SolidWorks and AutoCAD are used to model the structure and the complete arrangement. ARDUINO is used for the simulation of valve operation as a microcontroller simulator.

When analyzing the results, considering the pilot model, the captured practical power output was 19.9 W on average and 48.5 W at its maximum. Whereas the theoretically calculated maximum power output for the pilot model is 55.1 W. Since the theoretical calculations were based on several assumptions for energy efficiencies and ideal operational conditions, there is a slight deviation between the theoretical and practical values. Out of the results obtained, the overall efficiency of the complete system is around 4%. The main reason for the major loss is due to a large number of energy conversion stages throughout the entire process. However, by fine-tuning the energy conversion methods of these nodes, the overall losses can be minimized.

Mainly, if the source site selected had a higher wave height with higher wave energy, the amount of energy extraction would have been increased. Referring to Figure 2.1, the locations around the North Pole and the South Pole have the highest wave heights [4]. In Sri Lanka, the Southern Sea has higher wave heights. Therefore, the average efficiency of this model is directly proportional to the wave power capacity of the selected site.

Further, as per the research study, when considering the energy conversion process of the complete system and the construction of the pilot model, there are many energy-loss points throughout. Under the project progress review, such identified points were addressed with proven records. As an example, one of the main energy loss points was at the air discharge section. To harness the maximum energy from the air output, the number of blades was increased, and the turbine blades were enclosed to minimize the air losses. That approach successfully mitigated the loss to a reasonable extent.

However, the main objective of the research was to develop a system to generate 1 kW out of 1 m^2. Initially, this objective was followed on the basis of literature reviews with the available energy capacity of the waves. Although there is a theoretical possibility of achieving that objective with the existing wave energy, practically, that could not be reached due to the above-mentioned losses and ideal operational conditions. Since this is a pilot project where there was no exactly similar system to study, the complete system was designed based on the basic principles. Now, from this point onwards, it is easier to develop the system to have a higher efficiency by addressing the losing nodes, with reference to the energy flow diagram.

The energy storage concept (CAES) proposed in this research has claimed a major loss in system efficiency. As per the energy flow diagram, the loss is 88%, which was expected to reach 50% at the target outcomes. However, the study has proven the ability of energy storage as compressed air, which can be discharged on demand. Hence, the compressed air cylinders can be used to store energy.

As a summary, this system was proposed to generate 1 kW out of a 1 m^2 area of sea wave surface, where there is a wave power capacity of 1.44 kW/m^2 to a wave height of 2.1 m, wave period of 10 s, and wave front of 15 m. With the selected method of energy extraction to generate electricity, there were several energy losses along with the energy flow from the available resources. Hence, the ultimate efficiency has ended up at 4%, which was expected to be 8% based on the research outcomes. Finally, referring to the above calculations for the theoretical model and the pilot model, the ultimate objective of the research has been reached to an acceptable extent, where the electricity can be generated from sea wave energy, and the extracted energy from the sea waves can be stored as compressed air for future usage.

7.2 Recommendations

As described in the above section, the complete system has been tried out with different approaches to simulate the design with the actual data. It would be more convenient if the complete simulation could be performed on a single platform. But, due to several technical and financial impacts, some of the available simulation models are out of reach. However, as an initial step in the wave energy extraction to store and generate electricity as a renewable energy development, I hope the proposed approach will help to validate the research objectives.

The efficiency of the complete system could be improved if the losses at air compression (30%) and air discharge at the accumulator (88%) could be minimized. For that, further studies can be done on air compressions and discharging to reduce losses by modifying the air turbine. Such actions can be taken to mitigate losses. Moreover, the input air for the compression can be heated by interacting with solar thermal energy to increase the efficiency of air compression.

When considering the electricity generation, the recorded output was not a continuous delivery. The output mainly depends on the air pressure and the rate of air discharge. Since the air discharging of the pilot model was operated with only two accumulators, it can be stabilized by a series of accumulators linked in a network, as mentioned in Section 3.11 of Chapter 3.

Finally, as this is a novel concept, extended studies can be conducted beyond this research to develop the existing wave energy resource for the sustainability of the future world.

REFERENCES

[1] G. Mork, S. Barstow, A. Kabuth, and M. T. Pontes, "Assessing the global wave energy potential," in *International Conference on offshore mechanics and arctic engineering*, 2010, pp. 447–454. Accessed: May 26, 2025. [Online]. Available: https://asmedigitalcollection.asme.org/OMAE/proceedings-abstract/OMAE2010/447/345942

[2] K. Gunn and C. Stock-Williams, "Quantifying the global wave power resource," *Renew. Energy*, vol. 44, pp. 296–304, 2012.

[3] A. F. de O. Falcão, "Wave energy utilization: A review of the technologies," *Renew. Sustain. Energy Rev.*, vol. 14, no. 3, pp. 899–918, 2010.

[4] R. Waters, "Energy from ocean waves: full scale experimental verification of a wave energy converter," PhD Thesis, Universitetsbiblioteket, 2008. Accessed: May 26, 2025. [Online]. Available: https://www.diva-portal.org/smash/record.jsf?pid=diva2:172943

[5] M. E. McCormick, *Ocean wave energy conversion*. Courier Corporation, 2013. Accessed: May 26, 2025. [Online]. Available: https://books.google.com/books?hl=en&lr=&id=wkDDAgAAQBAJ&oi=fnd&pg=PP11&dq=M.+E.+McCormick,+Ocean+Wave+Energy+Conversion.+Mineola,+NY:+Dover+Publications,+2013&ots=we-h8CZ1an&sig=vREdGsaK9GTfoxs3cxOEhVWV_I4

[6] A. Babarit, "A database of capture width ratio of wave energy converters," *Renew. Energy*, vol. 80, pp. 610–628, 2015.

[7] M. Z. A. Khan, H. A. Khan, and M. Aziz, "Harvesting Energy from Ocean: Technologies and Perspectives," *Energies*, vol. 15, no. 9, p. 3456, May 2022, doi: 10.3390/en15093456.

[8] "Perth Wave Energy Project," Power Technology. Accessed: May 26, 2025. [Online]. Available: https://www.power-technology.com/projects/perth-wave-energy-project/

[9] R. Henderson, "Design, simulation, and testing of a novel hydraulic power take-off system for the Pelamis wave energy converter," *Renew. Energy*, vol. 31, no. 2, pp. 271–283, 2006.

[10] R. Yemm, D. Pizer, C. Retzler, and R. Henderson, "Pelamis: experience from concept to connection," *Philos. Trans. R. Soc. Math. Phys. Eng. Sci.*, vol. 370, no. 1959, pp. 365–380, Jan. 2012, doi: 10.1098/rsta.2011.0312.

[11] A. R. Lesemann and E. J. Hammagren, "Searay Autonomous Offshore Power System AOPS: Results of Sea Trials and Payload Support

Demonstration," Accessed: May 26, 2025. [Online]. Available: https://dx.doi.org/10.4043/31042-MS

[12] D. Mollison, O. P. Buneman, and S. H. Salter, "Wave power availability in the NE Atlantic," *Nature*, vol. 263, no. 5574, pp. 223–226, 1976.

[13] J. A. Rea, D. B. Murray, K. Leyne, and S. Armstrong, "Electrical Design Considerations for Islanded Power Platform for Wave Energy Test Sites".

[14] A. de O. Falcão, "The development of wave energy utilisation," *Glob. Status Crit. Dev. Ocean Energy*, p. 15, 2008.

[15] D. Curto, V. Franzitta, and A. Guercio, "Sea Wave Energy. A Review of the Current Technologies and Perspectives," *Energies*, vol. 14, no. 20, Art. no. 20, Jan. 2021, doi: 10.3390/en14206604.

[16] T. V. Heath, "The development and installation of the LIMPET Wave Energy Converter," in *World renewable energy congress VI*, Elsevier, 2000, pp. 1619–1622. Accessed: May 26, 2025. [Online]. Available: https://www.sciencedirect.com/science/article/pii/B9780080438658503342

[17] P. Frigaard, J. P. Kofoed, and J. W. Tedd, "The Wave Energy Device: The International Interdisciplinary Conference on Sustainable Technologies for Environmental Protection (ICSTEP 2006)," *Proc. Int. Interdiscip. Conf. Sustain. Technol. Environ. Prot.*, 2006.

[18] H. C. Soerensen *et al.*, "Development of Wave Dragon from Scale 1:50 to Prototype: The Fifth European Wave Energy Conference," *Proc. Fifth Eur. Wave Energy Conf.*, vol. Session 11, 2003.

[19] S. S. Prakash *et al.*, "Wave Energy Converter: A Review of Wave Energy Conversion Technology," in *2016 3rd Asia-Pacific World Congress on Computer Science and Engineering (APWC on CSE)*, Nadi, Fiji: IEEE, Dec. 2016, pp. 71–77. doi: 10.1109/APWC-on-CSE.2016.023.

[20] P. Beirão, "Modelling and control of a wave energy converter: Archimedes wave swing," *Inst. Super. Téc. Lisb. Portigal*, 2007, Accessed: May 26, 2025. [Online]. Available: https://www.researchgate.net/profile/Pedro-Beirao-2/publication/247160804_Modelling_and_Control_of_a_Wave_Energy_Converter_Archimedes_Wave_Swing/links/5731f71108ae9ace8404753b/Modelling-and-Control-of-a-Wave-Energy-Converter-Archimedes-Wave-Swing.pdf

[21] D. Valério, P. Beirão, and J. Sá da Costa, "Optimisation of wave energy extraction with the Archimedes Wave Swing," *Ocean Eng.*, vol. 34, no. 17, pp. 2330–2344, Dec. 2007, doi: 10.1016/j.oceaneng.2007.05.009.

[22] J. P. Kofoed, P. Frigaard, and M. Kramer, "Recent developments of wave energy utilization in Denmark," in *Proceedings of the Korea Committee for Ocean Resources and Engineering Conference*, Korean Society of Ocean

Engineers, 2006, pp. 91–98. Accessed: May 27, 2025. [Online]. Available: https://koreascience.kr/article/CFKO200611764899324.page

[23] M. Kramer, "Performance evaluation of the wavestar prototype," in *9th ewtec 2011: Proceedings of the 9th European Wave and Tidal Conference, Southampton, UK, 5th-9th September 2011*, University of Southampton, 2011. Accessed: May 27, 2025. [Online]. Available: https://vbn.aau.dk/en/publications/performance-evaluation-of-the-wavestar-prototype

[24] A. Parwal *et al.*, "Wave Energy Research at Uppsala University and The Lysekil Research Site, Sweden : A Status Update," presented at the Proceedings of the 11th European Wave and Tidal Energy Conference. Nantes, France, September 2015, 2015. Accessed: May 27, 2025. [Online]. Available: https://urn.kb.se/resolve?urn=urn:nbn:se:uu:diva-265218

[25] T. Aderinto and H. Li, "Review on power performance and efficiency of wave energy converters," *Energies*, vol. 12, no. 22, p. 4329, 2019.

[26] V. A. U. De Alwis, A. P. K. De Silva, S. Gunawardane, and Y.-H. Lee, "Computational fluid dynamic simulation of hull reservoir wave energy device," in *Journal of Physics: Conference Series*, IOP Publishing, 2022, p. 012041. Accessed: May 27, 2025. [Online]. Available: https://iopscience.iop.org/article/10.1088/1742-6596/2217/1/012041/meta

[27] D. H. Robison and P. J. Beaty, "Compressor Types, Classifications, And Applications.," 1992, Accessed: May 27, 2025. [Online]. Available: https://hdl.handle.net/1969.1/163528

[28] C. Borzea *et al.*, "Compressed air energy storage installation for renewable energy generation," in *E3S Web of Conferences*, EDP Sciences, 2019, p. 02010. Accessed: May 27, 2025. [Online]. Available: https://www.e3s-conferences.org/articles/e3sconf/abs/2019/38/e3sconf_te-re-rd18_02010/e3sconf_te-re-rd18_02010.html

[29] M. Takao and T. Setoguchi, "Air Turbines for Wave Energy Conversion," *Int. J. Rotating Mach.*, vol. 2012, no. 1, p. 717398, 2012, doi: 10.1155/2012/717398.

[30] F. Lopez Gomez Partida, *Design of a Permanent Magnet Synchronous Generator with Alnico Magnets*. 2019. Accessed: May 27, 2025. [Online]. Available: https://urn.kb.se/resolve?urn=urn:nbn:se:uu:diva-395215

[31] R. K. Rajput, *Thermal Engineering*. Firewall Media, 2005.

[32] M. U. V. Mane and M. S. S. Choure, "DESIGN AND STRUCTURAL ANALYSIS OF PELTON WHEEL TURBINE BLADE," *Int. J.*, vol. 5, no. 12, 2020, Accessed: May 27, 2025. [Online]. Available: https://www.ijasret.com/VolumeArticles/FullTextPDF/609_3.DESIGN_AND

_STRUCTURAL_ANALYSIS_OF_PELTON_WHEEL_TURBINE_BLADE.pdf

[33] A. De Vos, C. B. Pattiaratchi, and E. M. S. Wijeratne, “Surface circulation and upwelling patterns around Sri Lanka,” *Biogeosciences*, vol. 11, no. 20, pp. 5909–5930, 2014.

Appendix 1: Climate seasons and wind patterns of Sri Lanka

Climate seasons are experienced annually

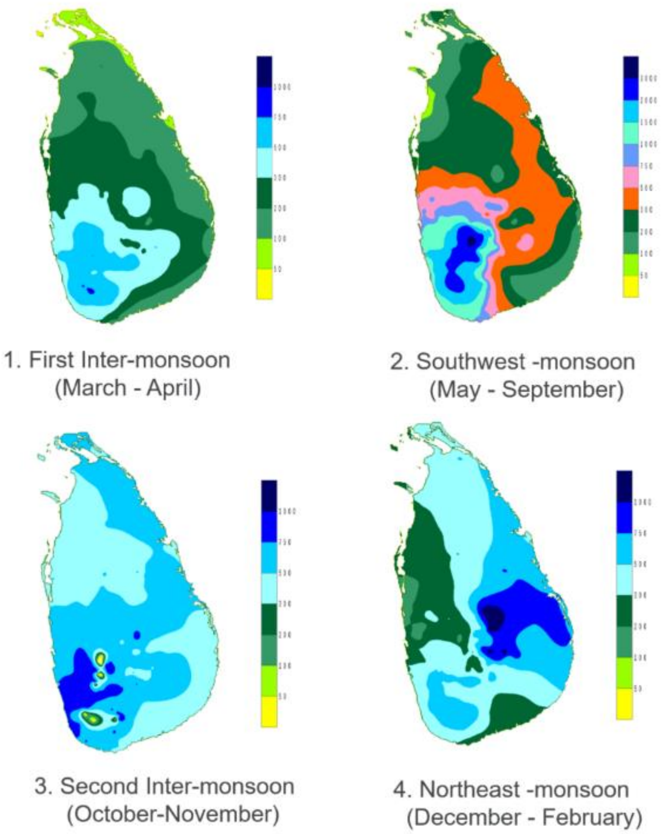

Figure A1.1: Climate seasons of Sri Lanka: www.meteo.gov.lk

Wind directions of Sri Lanka [33]

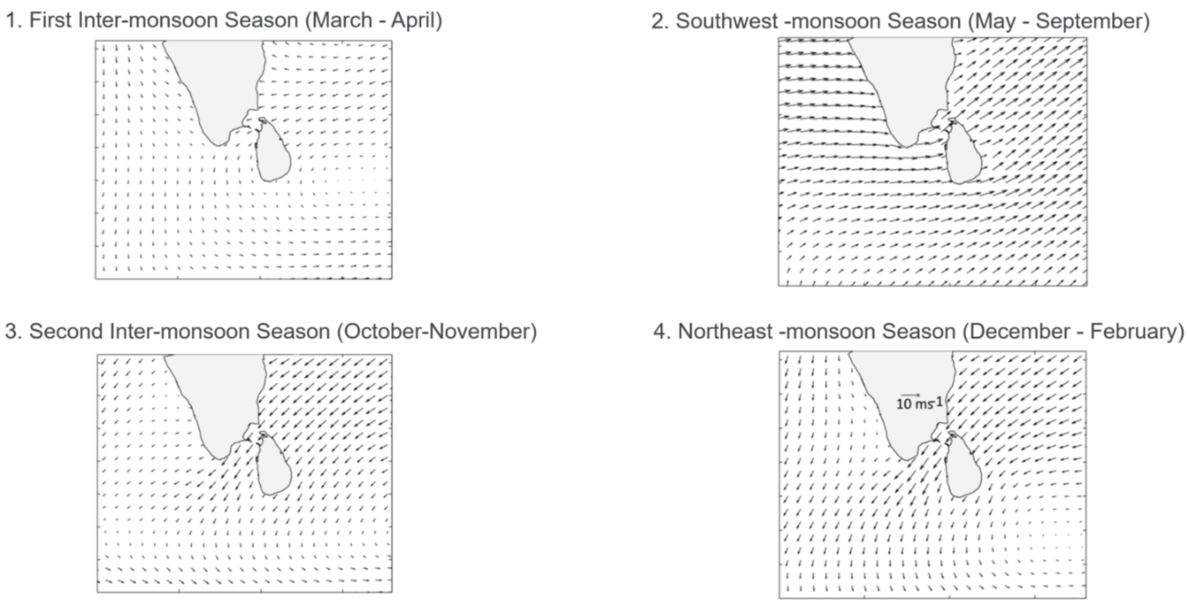

Figure A1.2: Wind patterns of Sri Lanka

Appendix 2: Wind speed and wave height variation

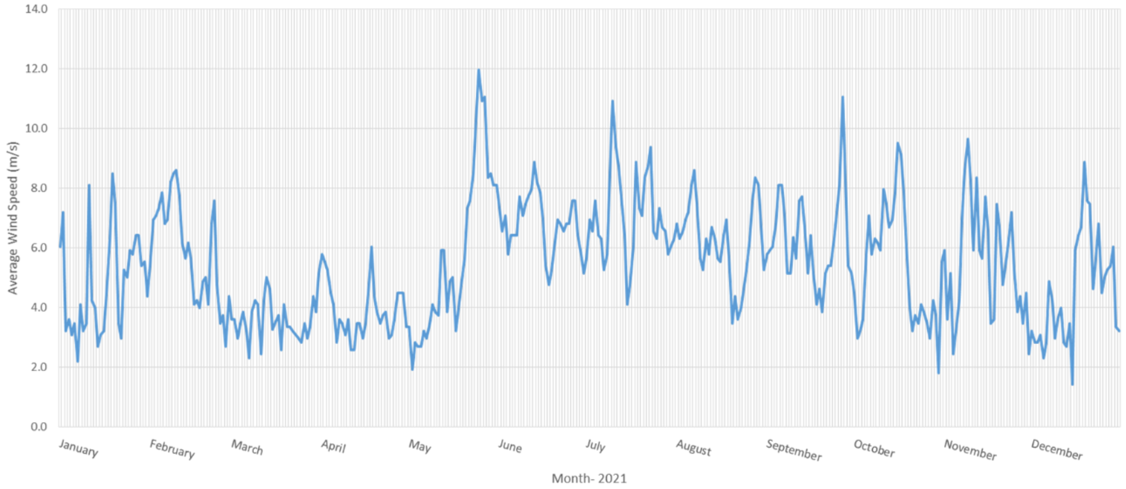

Figure A2.1: Wind speed variation – Colombo www.windguru.cz

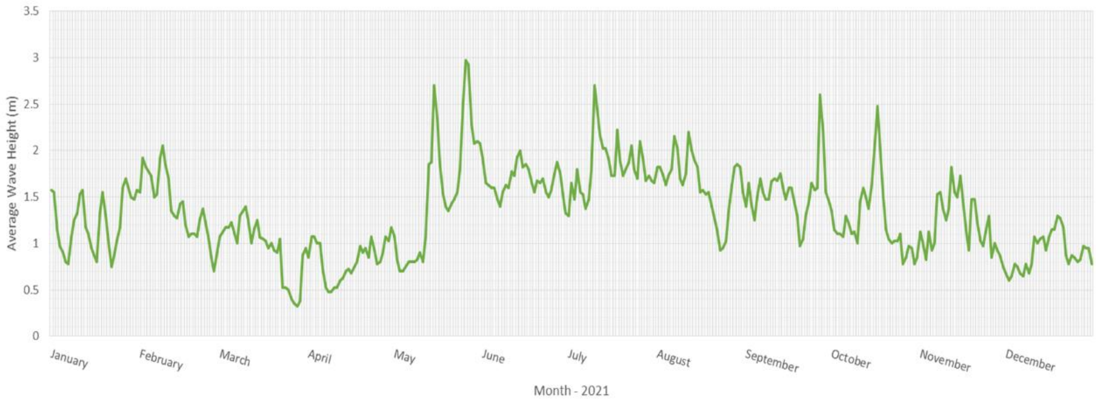

Figure A2.2: Wave height variation – Colombo www.windguru.cz

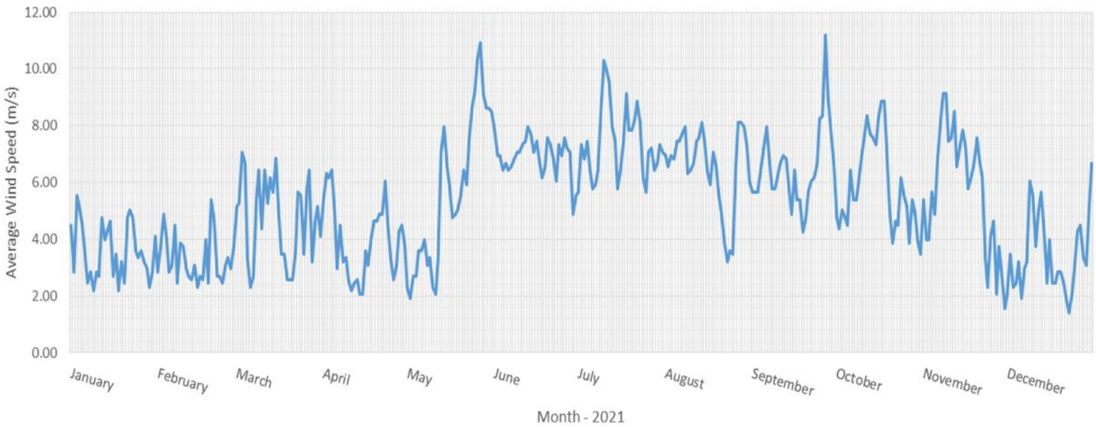

Figure A2.3: Wind speed variation – Weligama www.windguru.cz

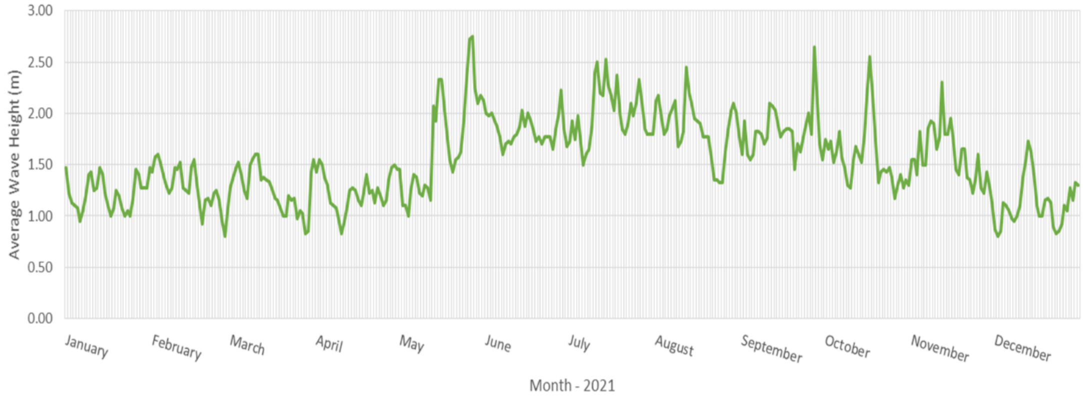

Figure A2.4: Wave height variation – Weligama www.windguru.cz

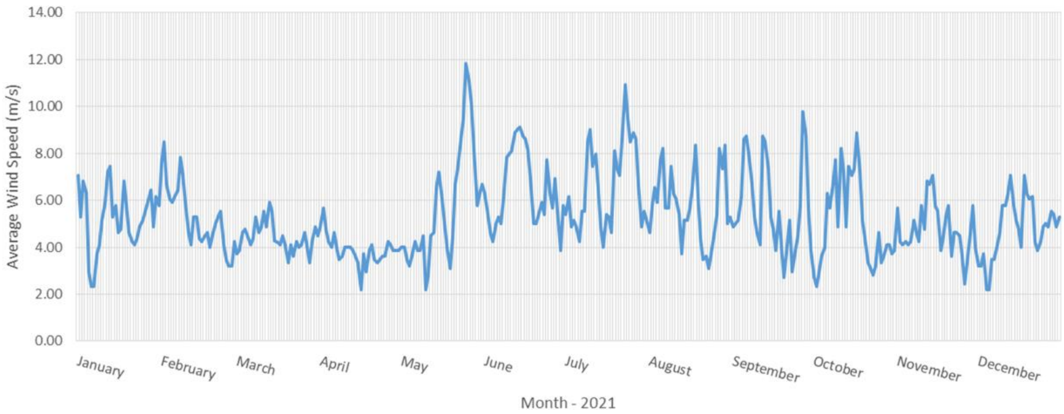

Figure A2.5: Wind speed variation – Trincomalee www.windguru.cz

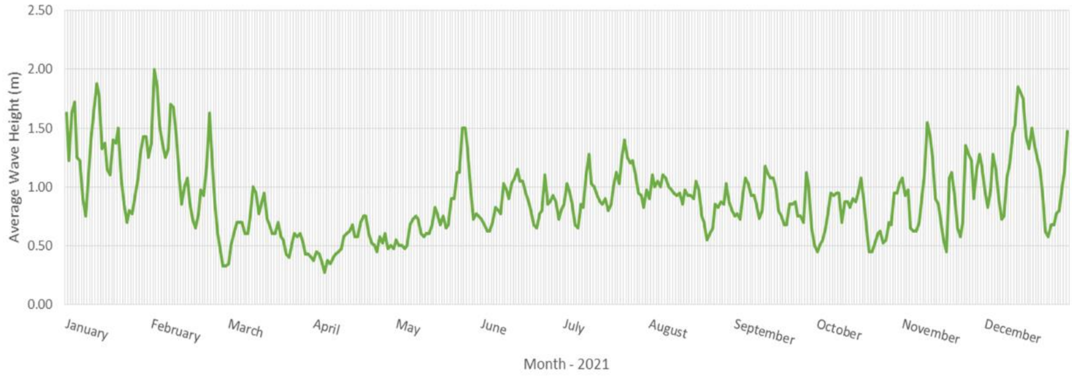

Figure A2.6: Wave height variation – Trincimalee www.windguru.cz

Appendix 3: Arduino code

```
int RelaypinA= 3;
int RelaypinB= 5;
int RelaypinC= 6;
int RelaypinD= 10;

void setup() {
pinMode(RelaypinA, OUTPUT);
pinMode(RelaypinB, OUTPUT);
pinMode(RelaypinC, OUTPUT);
pinMode(RelaypinD, OUTPUT);
}

void loop() {
digitalWrite(RelaypinA, HIGH);
digitalWrite(RelaypinB, LOW);
digitalWrite(RelaypinD, HIGH);
digitalWrite(RelaypinC, LOW);
delay(60000);

digitalWrite(RelaypinA, LOW);
digitalWrite(RelaypinB, HIGH);
digitalWrite(RelaypinD, LOW);
digitalWrite(RelaypinC, HIGH);
delay(60000);
}
```

Appendix 4: Specifications of the Permanent Magnet Generator

Specifications - Permanent Magnet 3 Phase Low RPM Generator

Model Number	BM-1000
Type	3 Phase Permanent Magnet Wind Generator
Rated Power	1000W
Rated Voltage	12VAC
Rotate Speed	300 RPM
Generator case	Aluminium alloy
Shell Material	Aluminium alloy
Shaft material	: Stainless steel
Permanent Magnet Material,	Rare Earth NdFeB
Protection Grade	IP55
Origin	Mainland China
Certification	CE

Figure A4.1: Permanent magnet AC generator

Appendix 5: Load Test Report

Table A5.1: Load test report

Case 1 - 100W Halogen Bulb x 2			
RPM	**A**	**V**	**W**
651	0.63	0.19	0.120
651	0.64	0.18	0.115
651	0.64	0.18	0.115
651	0.64	0.18	0.115
651	0.64	0.18	0.115

Case 2 - 21W Filament Bulb x 5			
RPM	**A**	**V**	**W**
983	4.25	2.4	10.200
983	0.99	8.3	8.217
774	4.38	2	8.760
774	4.38	2	8.760
654	0.51	14.8	7.548

Case 3 - 21W Filament Bulb x 4			
RPM	**A**	**V**	**W**
856	0.52	25.6	13.312
856	4.63	2.8	12.964
673	3.69	1.2	4.428
302	3.46	5.4	18.684
302	0.48	5.4	2.592

Case 4 - 21W Filament Bulb x 3			
RPM	**A**	**V**	**W**
955	4.01	12.1	48.521
955	0.37	12.1	4.477
797	3.39	7	23.730
797	1.27	5.5	6.985
467	0.35	15.3	5.355

Case 5 - 21W Filament Bulb x 2			
RPM	**A**	**V**	**W**
1456	2.29	6.9	15.801
1397	3.2	7.7	24.640
1384	2.4	7.6	18.240
942	1.24	18.2	22.568
942	2.28	8.1	18.468

Case 6 - 21W Filament Bulb x 1			
RPM	**A**	**V**	**W**
591	1.99	14.1	28.059
591	1.55	9.1	14.105
321	1.8	10.8	19.440
321	1.39	12.4	17.236
321	1.4	10.8	15.120

Case 7 - 21W Filament Bulb x 1			
RPM	**A**	**V**	**W**
211	2.27	10.5	23.835
211	1.35	14.2	19.170
211	1.82	8.5	15.470
211	1.15	12.5	14.375
211	1.22	10.5	12.810

Appendix 6: MATLAB code for sea wave motion

```
% Constants
g = 9.81; % acceleration due to gravity, m/s^2

% Given data
average_wave_height = 0.89; % meters
maximum_wave_height = 2.1; % meters
average_wind_speed = 5.31; % m/s
vertical_displacement_wave = 0.625/2; % meters
buoyant_force = 5000; % N
wave_frequency = 0.25; % Hz

% Time settings
time_step = 0.1; % seconds
total_time = 30; % seconds
time_points = 0:time_step:total_time;
num_time_points = length(time_points);

% Simulate the vertical motion
vertical_displacement = zeros(1, num_time_points);

for t = 1:num_time_points
    wave_height = average_wave_height + (maximum_wave_height - average_wave_height)
* rand(); % Assuming a random wave height
    wave_period = 1 / wave_frequency; % Wave period calculation
    wave_phase = 2*pi * time_points(t) / wave_period; % Wave phase based on time

    wave_displacement = vertical_displacement_wave * sin(wave_phase); % Vertical
displacement due to wave
    total_displacement = wave_displacement + buoyant_force / (buoyant_force /
vertical_displacement_wave); % Total vertical displacement

    vertical_displacement(t) = total_displacement;
end

% Plot the results
figure;
plot(time_points, vertical_displacement);
xlabel('Time (s)');
ylabel('Vertical Displacement (m)');
title('Vertical Motion of Floater');
grid on;
```

Appendix 7: MATLAB code for pressurization of piston cylinder

```
% Given data
tank_capacity = 24; % liters
fill_time = 5.03 * 60; % seconds
pressure = 10; % bar
piston_volume = 318; % cm^3
piston_displacement = 31.67; % cm
piston_frequency = 0.25; % Hz

% Calculations
piston_area = piston_volume / piston_displacement; % Piston cross-sectional area
tank_volume = tank_capacity * 1000; % Convert liters to cm^3
tank_cross_sectional_area = tank_volume / piston_displacement; % Tank cross-sectional
area

% Time settings
total_time = fill_time; % Fill one tank
time_points = linspace(0, total_time, 1000);

% Calculate pressure increment in the tank over time
pressure_increment = zeros(size(time_points));

for i = 1:length(time_points)
    t = time_points(i);

    % Calculate piston position and pressure based on piston's sinusoidal motion
    piston_position = piston_displacement * sin(2*pi*piston_frequency*t);
    current_pressure = pressure * (piston_displacement - piston_position) /
piston_displacement;

    % Calculate volume of air added to the tank during this time step
    air_volume_added = piston_area * abs(piston_position); % Ensure positive volume

    % Calculate pressure increment in the tank
    pressure_increment(i) = current_pressure * (air_volume_added /
tank_cross_sectional_area);
end

% Plot pressure increment in the tank
figure;
plot(time_points, pressure_increment, 'b', 'LineWidth', 1.5);
xlabel('Time (s)');
ylabel('Pressure Increment (bar)');
title('Pressure Increment in the Tank');
grid on;
```

Appendix 8: MATLAB code for pressure variation at Pelton turbine

```
% Given data
P0 = 7.5;         % Initial pressure (in bar)
tau = 5.03;       % Time constant for decay (in minutes)
time_intervals = 6;
interval_duration = 5.03;  % minutes

% Generate time points
time_points = linspace(0, time_intervals * interval_duration, 1000);  % More points for
smoother plot

% Initialize pressure_values array
pressure_values = zeros(1, length(time_points));

% Iterate over intervals
for i = 1:time_intervals
    % Calculate pressure decay within the interval
    decay_indices = (time_points >= (i - 1) * interval_duration) & (time_points <= i *
interval_duration);
    pressure_values(decay_indices) = P0 * exp(-(time_points(decay_indices) - (i - 1) *
interval_duration) / tau);

    % Calculate pressure rise within the interval
    rise_indices = (time_points > (i - 1) * interval_duration + tau) & (time_points <= i *
interval_duration - tau);
    pressure_values(rise_indices) = P0;

    % Calculate pressure decay after the rise
    pressure_values(rise_indices) = pressure_values(rise_indices) .* exp(-
(time_points(rise_indices) - i * interval_duration + tau) / tau);
end

% Plot the graph
figure;
plot(time_points, pressure_values, 'b');
xlabel('Time (minutes)');
ylabel('Pressure (bar)');
title('Turbine Blade Air Pressure Variation');
grid on;

% Set y-axis limits
ylim([1, 10]);

% Display the plot
disp('Turbine Blade Air Pressure Variation Plot:');
```